INT. REVIEWS IN PHYSICAL CHEMISTRY, 2003
VOL. 22, NO. 4, 593–640

Taylor & Francis
Taylor & Francis Group

Size-dependent reactivity in open shell metal-ion polar solvent clusters: spectroscopic probes of electronic-vibration coupling, oxidation and ionization

JAMES M. FARRAR†
Department of Chemistry, University of Rochester, Rochester, NY 14627, USA

This review considers the spectroscopy and structure of clusters formed by stepwise addition of polar solvent molecules such as NH_3, H_2O, and CH_3OH to effective one-electron chromophores that include the singly-charged alkaline earth cations Mg^+, Ca^+, and Sr^+; atomic sodium; and the Rydberg molecule NH_4. The absorption of photons by such species results in initial electronic excitation, followed by energy transfer to vibrational degrees of freedom, ultimately leading to dissociation. Experimental data are presented to support this electronic-to-vibrational energy transfer mechanism. Wavelength-dependent photodissociation signals for all of these species exhibit a similar size-dependence in which large spectral red shifts are observed as the first solvation shell fills. An examination of *ab initio* calculations on a number of related systems, as well as theoretical models for charge transfer, suggests that non-covalent interactions of solvent molecules with the single valence electron of the cluster core lead to spontaneous ionization of the core with increasing cluster size. The process is analogous to the formation of solvated electrons in condensed phases. The collective results suggest that within the broad topic of solvation and the formation of solutions, clusters can provide a linkage between the properties of the gas phase and those of condensed phases.

Contents

†E-mail: farrar@chem.rochester.edu

International Reviews in Physical Chemistry ISSN 0144–235X print/ISSN 1366–591X online
http://www.tandf.co.uk/journals
DOI: 10.1080/01442350310001616896

1. Introduction

In recent years, the state of matter referred to as clusters has received significant theoretical and experimental attention. Clusters consist of finite aggregates of weakly-bound species held together by non-covalent interactions. As paradigms for the study of dynamical processes in finite systems with a small number of degrees of freedom, and as models to probe the evolution of the properties of condensed phases from their monomeric constituents, research on clusters has generated a very large literature [1–6]. Clusters are often touted as the bridges between the gas and condensed phases [7], but those bridges are often very long and sometimes poorly mapped. For example, the development of the bulk work function of a metal from the ionization potentials of isolated atoms via small clusters has demonstrated the need for experimental data for clusters up to a size range where precise mass selection and size characterization is quite difficult to achieve [8, 9]. Several research studies have also demonstrated that in some systems, the properties of clusters are unique to that specific state of matter, rather than providing insight into transitions among distinct phases [10–13]. Of all the condensed matter properties that have been probed with some degree of size-selectivity, ion solvation stands out as a process that proceeds from gas to bulk on a length scale sufficiently compact that it can be probed effectively over a narrow range of cluster sizes [14, 15]. In part, this state of affairs arises from the fact that the volume associated with the short Debye length characteristic of the range of ionic interactions in dilute electrolyte solutions can accommodate a relatively small number of solvent molecules. Consequently, studies of the structures of small metal ion–solvent complexes and the size-dependences of dynamical processes occurring in those clusters have significant potential to illuminate the properties of metal ions in the condensed phase. Such systems may also serve as paradigms for unravelling the intrinsic properties of collisional energy transfer and chemical processes such as proton and electron transfer from the ensemble averaging inherent in condensed phases.

Metal ions and their complexes play a central role in many chemical processes, both in the condensed phase and in small aggregates. The role of these species makes an understanding of their structures and dynamical processes over a range of sizes fundamental to many important questions in solution chemistry, catalysis, and materials chemistry. The nature of the non-covalent interactions that occur between metal ions and solvents plays an important role in the ability of biologically active molecules to assume the conformations required to carry out selective chemical processes [16]. Metal ion complexes also play a role in many environmental problems, including metal speciation and atmospheric processes involving metal ion-based aerosols. Electron transfer between metal and ligand often controls the nature of electronic transitions in such complexes, and therefore the electronic and optical properties of materials based on such simple systems [17].

The fundamental role played by ion solvation in this diverse set of problems has led to intense experimental and theoretical activity to understand the structural and dynamical aspects of the process. In particular, gas phase spectroscopy of mass-selected metal ion–solvent complexes has played a critical role in developing our understanding of these fundamental processes at the most elementary level. Mass spectrometry and optical spectroscopy of size-selected cluster ions are important methods for understanding solvation phenomena, especially the manner in which each successive solvent molecule contributes to the establishment of the properties of bulk solutions [1]. A significant amount of research employing vibrational spectroscopy on size-selected clusters of closed-shell singly-charged ions, i.e. the alkali ions, solvated by H_2O and CH_3OH, has provided evidence for the formation of a second solvation shell before the first shell has coordinated fully [18]. Closed-shell ions, while interesting in their own right, provide only a limited perspective on solvent shell formation based on steric and electrostatic factors.

Probes of the interactions between open-shell ions and solvent molecules offer additional opportunities to assess solvation in physically realizable bulk systems. However, the study of such systems introduces additional challenges, many of which arise from the existence of more than one oxidation state of the metal. The alkaline earth systems provide a case in point. The singly-charged alkaline earth ions, e.g. Mg^+, Ca^+, and Sr^+, represent examples of systems that do not occur naturally in condensed phase systems, but nonetheless provide insight into the ion–molecule interactions that ultimately lead to solvation. The electronic transitions of the single valence electron in these species provide a convenient probe of the local solvation environment around the ion. Recently, Stace [15] has pointed out the importance of observing the higher oxidation states of clusters formed from polar solvent molecules with alkaline earth ions, and has also commented on the difficulties associated with producing such species. The well-known reactivities of these ions with the solvent H_2O to form the metal hydroxides, or with CH_3OH to form metal methoxides and hydroxides, illustrate the propensity of these species to access the higher 2+ oxidation state even in clusters. The coupling of the electronic energy of the atomic ion core with reactive processes involving solvent degrees of freedom [19–21] provides critical opportunities for probing structural and dynamical features of the solvation process. The excitation energies of electronic states based on the strongly-allowed valence transitions in the alkaline earth ions exceed their electrostatic binding energies with polar solvents [22, 23] such as NH_3, H_2O, CH_3OH, and CH_3NH_2; consequently, those couplings can lead to dissociation by cleavage of specific bonds within the solvent and by the simpler process of solvent evaporation [24–33]. Those processes can occur both on excited state surfaces and on the ground state surface following internal conversion.

The local electronic environment of the metal ion valence electron provides detailed spectroscopic information about excited state and ground state dynamics, probing the solvation process at the level of the potential energy surfaces that govern motions on the atomic length scale. Singly-charged alkaline earth cations are isoelectronic with alkali atoms, and thus a study of the evolution of electronic structure in the vicinity of the atomic centre may also provide insight into the process of spontaneous ionization and formation of solvated electrons. This topic continues to occupy the efforts of experimentalists and theoreticians today [34, 35].

In this review article, we discuss recent studies of the electronic structure and reaction dynamics of alkaline earth cations bound to variable numbers of polar

solvent molecules as probed in gas phase photodissociation experiments with size-selected cluster ions. We will discuss results from several different systems, ranging from those that simply evaporate solvent molecules after internal conversion to the ground state surface of the system, to systems in which strong coupling between electronic and vibrational degrees of freedom results in formation of covalent bonds between the metal and atoms of the solvent. The review will focus not only on the wavelength-dependence of the total photodissociation signal for mass-selected clusters as a function of size, but also on cluster size dependent branching ratios for systems that have several competitive reaction channels. These latter studies address directly the nature of the metal oxidation processes in clusters. Parallels between the photodissociation signals in mass-selected clusters ions and neutral species built on a 'core' that is isoelectronic with singly-charged alkaline earth cations, e.g. alkali atoms and the Rydberg radical NH_4, will also be discussed. This review will focus on the evolution of cluster properties as a function of the number of bound polar solvent molecules. Therefore, a number of interesting topics, including high resolution spectroscopy [20, 21, 36] and studies of metal ion–rare gas complexes [37–51] will therefore not be covered in this article. The experimental results will also be discussed in the context of *ab initio* calculations that explore ground state geometries, excited state energetics, and electron density distributions in ground and excited states.

2. Experimental methods

The experimental apparatus employed in this work is similar in design to systems in the laboratories of a number of investigators, and is shown in figure 1 [52–58]. The instrument consists of a laser vaporization–supersonic expansion source [59] for producing clusters, a Wiley–McLaren time-of-flight mass spectrometer [60] for primary mass selection, a photolysis source, and a reflecting ion mirror ('reflectron') [61] for mass analysis of the photolysis products. A distribution of parent clusters is

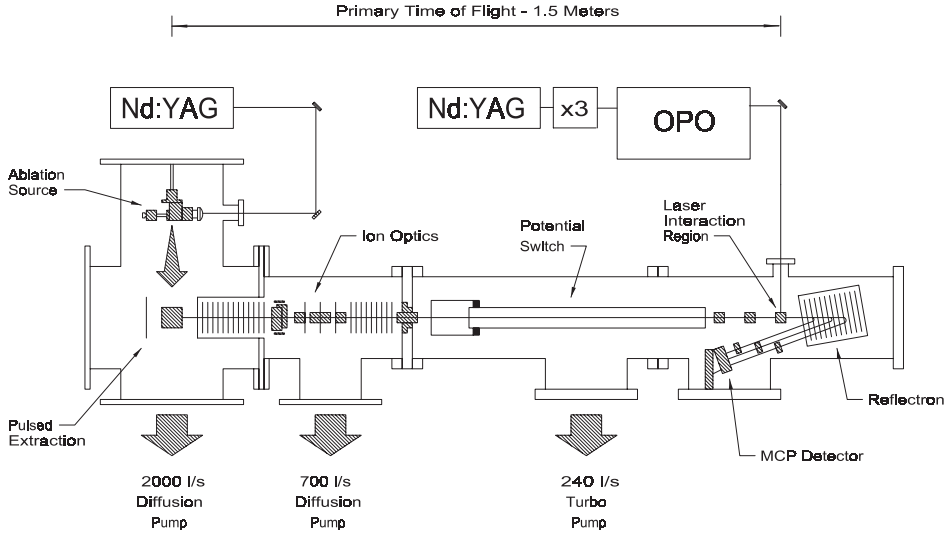

Figure 1. Schematic diagram of TOF-reflectron tandem mass spectrometer at the University of Rochester.

produced by 532 nm laser ablation of a disk of alkaline earth metal, the plasma from which is then entrained in a mixture of rare gas and solvent vapour and expanded into vacuum in the source region. The clusters are then extracted perpendicularly by a fast electrical pulse from a thyratron switch into the beam line and focused laterally in space to the laser interaction region downstream. The focal point is defined by the Wiley–McLaren conditions set by the extraction and acceleration potentials. The einzel lens corrects for beam divergence during transit to the detector. The acceleration potential gives the ions approximately equal energies, and thus flight times are directly proportional to the square root of the cluster mass. The parent ion packets are separated in time as they travel downstream through the field free flight tube. With a flight path of 1.5 m and a beam energy of 2000 eV, flight times for relevant masses will be on the order of tens of μs with packet separations of a few μs. By proper timing of the photolysis laser, any parent cluster packet can be chosen to interact with the laser pulse at the space focus of the packet.

The clusters are photolysed by radiation that intersects the cluster beam transversely at the spatial focus. This radiation is provided either by a Nd^{3+}:YAG-pumped dye laser or by a narrow bandwidth ($\sim 0.2\,cm^{-1}$) singly resonant optical parametric oscillator (OPO) (Spectra Physics, MOPO-730). The OPO signal wave tuning range is from 440–690 nm and its idler wave tuning range is from 730–1830 nm. The OPO is also equipped with a frequency doubler (FDO), allowing it to produce ultraviolet radiation. The FDO tunes from 220–345 nm by doubling signal frequencies and from 366–450 nm by doubling idler frequencies. The OPO is pumped by the third harmonic of an injection seeded Nd^{3+}:YAG laser (Spectra Physics, GCR-190) running at 10 Hz. Photodissociation creates a distribution of product and unphotolysed reactant ions, which are separated using a reflectron-type mass spectrometer. Photodissociation laser power is monitored throughout the experiment and kept at a constant value of 1 mJ/pulse.

The potential switch in the ion optics beam line changes the reference potential of the beam voltage from a few kilovolts to ground without changing the ion energy [58]. This technique allows the detection end of the instrument to be held at ground potential instead of floating at the initial beam voltage. The daughters produced after photolysis have nearly equal velocity and continue in the beam direction toward the reflectron, a reflecting field device. The reflectron is oriented at a slight angle to the beam line so that the ions follow a parabolic trajectory through it and are directed toward the microchannel plate (MCP) detector. Flight times through the reflectron are linearly dependent on mass, thus allowing the daughter ion packets to be separated in time as they arrive at the MCP. Signal from the particle detector is processed by a transient digitizer (DSP Corporation) and recorded as a function of laser wavelength by a computer. Timing and other instrument functions are accomplished by a CAMAC-based data acquisition system operated under computer control.

We measure the photodissociation signal by collecting photofragment product signals as a function of photolysis wavelength. In this work, as in many other examples, we equate the appropriately normalized photodissociation signal to the total absorption cross-section. Absolute photodestruction cross-sections are determined in the thin target limit from the following relation:

$$I/I_0 = \exp(-\sigma\Phi) \tag{1}$$

where I_0 and I are parent ion fluxes before and after laser irradiation respectively, σ is the photodestruction cross-section (units of cm^2) and Φ is the laser fluence (units of photon cm^{-2}). Charge conservation allows us to calculate the initial intensity of the parent ion, I_0, from the intensities of the daughter ions and residual parent ion. The shapes of size-dependent absorption cross-sections as a function of photon energy are reported in relative units, although it is possible to determine absolute cross-sections in favourable cases.

3. Parent ion mass spectra

Although the focus of the research is the electronic spectroscopy of size-selected clusters, it is informative to look at mass spectra of parent ions with various solvent molecules prepared by laser vaporization. Figure 2 shows the parent ion mass spectrum obtained for Sr^+ solvated by methanol [24, 27, 28] in which the hydrogen atom bound to oxygen is deuterium-labelled. The mass spectral intensity for a given solvent number is expected to be split into three lines because of the three naturally occurring isotopes of Sr. However, even for the $n=1$ cluster, the mass spectrum shows more than three lines, and careful analysis of the spectrum demonstrates that each group of lines is a superposition of intensities from cluster ions of molecular formulae $Sr^+(CH_3OD)_n$ and $SrCH_2OD^+(CH_3OD)_{n-1}$, in which a hydrogen atom bound to carbon is lost. The intensities of the latter group of ions grow with increasing cluster size until at $n=4$ solvent molecules, the C–H bond cleavage product is the dominant species in the mass spectrum. For the smallest clusters, there is no evidence to suggest that O–D bond cleavage occurs. In larger clusters, the data show evidence of loss of more than one hydrogen atom; although we cannot rule out O–D bond cleavage in these species, the data do not show abrupt

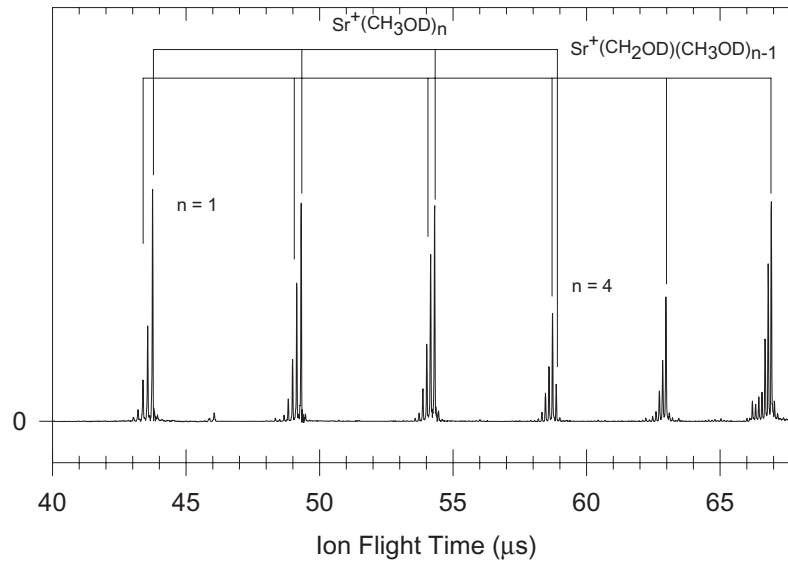

Figure 2. Parent mass spectra of $Sr^+(CH_3OD)_n$, for $n=1$ to 6. The spectrum illustrates formation of the series $Sr^+(CH_3OD)_n$ along with the series $Sr^+(CH_2OD)(CH_3OD)_{n-1}$, corresponding to H-loss from carbon. The latter series dominates the mass spectrum for the larger clusters. Figure reprinted from reference [28] with permission.

increases in intensity for clusters losing an even number of mass units, as would be expected if deuterium loss were to be a major reaction channel. The data are more readily explained in terms of C–H bond cleavages via unimolecular decay of nascent parent ions with the stoichiometry $Sr^+(CH_3OD)_k$. Similar behaviour is observed in parent $Mg^+(CH_3OD)_k$ clusters, i.e. preferential cleavage of C–H rather than O–H(D) bonds in ground state clusters [26].

The observation of C–H bond cleavage in the ground states of both $Sr^+(CH_3OD)_n$ and $Mg^+(CH_3OD)_n$ clusters can be rationalized on the basis of statistical decay of metastable complexes in which vibrationally excited solvent molecules activated in the laser vaporization process undergo unimolecular decay [62]. The mass spectrum of methanol shows that C–H bond cleavage occurs over O–H (or O–D) bond cleavage, a fact consistent with the lower bond strength of C–H bonds. Interestingly, however, both $Sr^+(CH_3OD)_n$ and $Mg^+(CH_3OD)_n$ show preferential cleavage of the O–D bond in the photodissociation process.

Cluster ions of Sr^+ solvated by NH_3 or ND_3 illustrate a different reactivity pattern than those formed with CH_3OD. The mass spectrum for $Sr^+(ND_3)_n$ clusters [54, 63] shows only a single species for solvent numbers in the range from 1 to 8. The intensity distribution goes through a local minimum near $n = 10$, but a secondary group of clusters peaking near $n = 12$ to 13 appears in the mass spectrum. Figure 3 shows a portion of the mass spectrum for $n = 12$ to 14, illustrating the formation of clusters with nominal stoichiometry $Sr^+(ND_3)_mD_x$, in which the number of *excess* deuterium atoms, x, can be as large as four. Fuke and co-workers have seen similar behaviour for clusters based on Mg^+, identifying clusters with one and two excess hydrogen atoms in the size range from $n \geq 6$ and $n \geq 10$ respectively [64, 65]. The interpretation of these mass spectra and spectroscopic probes of the $Sr^+(ND_3)_mD_x$ species will be presented in a later section of this article.

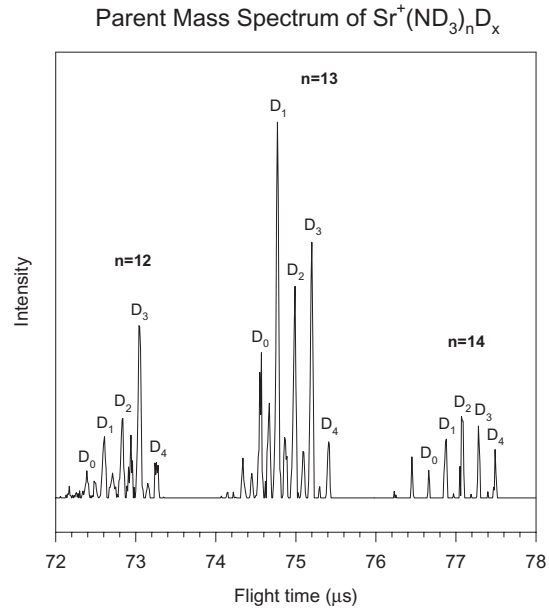

Figure 3. Parent ion mass spectrum for $Sr^+(ND_3)_nD_x$, for $n = 12$–14, $x = 0$–4. Figure reprinted from reference [63] with permission.

4. Photodissociation mass spectra

The TOF-reflectron instrument provides temporal separation of mass-selected parents and separation of daughter ions produced by photon absorption of a specific parent ion. Figure 4 shows a series of mass spectra taken at various wavelengths for $Sr^{+}(CH_3OD)_n$ clusters for $n = 1$ to 4 [27, 28]. Each of the spectra shows the intensity of residual parent ion belonging to the ^{88}Sr isotope and the

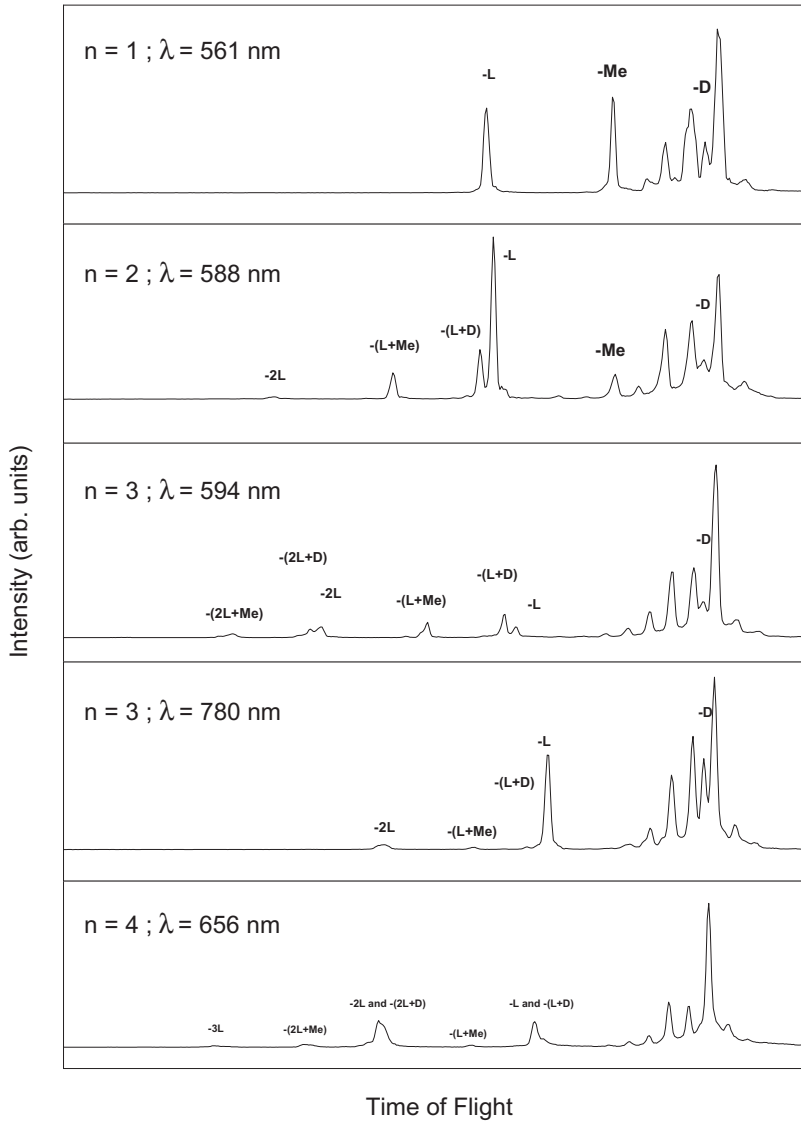

Figure 4. Dissociation of mass-selected 'parent' ion peak to create 'daughter' mass spectra at a single photolysis wavelength. We use the following shorthand notation to refer to the photolysis product peaks: –D = loss of deuterium atom, –Me = loss of a methyl fragment, –L = loss of an entire ligand. Combinations of these loss channels are denoted by the symbols listed combined with a + sign. In the case of multiple ligand loss, a coefficient equal to the number of lost ligands precedes the L symbol. Figure reprinted from reference [28] with permission.

unselected parent clusters of the ^{87}Sr and ^{86}Sr isotopes, along with the signals of primary product ions denoted by –D, –Me, and –L. This symbolism denotes the fragments lost by the parent cluster. The second panel of this figure shows the primary products for the $n=2$ cluster, but also shows another group of fragment ions in which the primary parents are accompanied by an additional solvent molecule. We refer to such products as combination channels. For example, the channel denoted –(L + D) corresponds to loss of a single solvent molecule plus a D atom. The third panel shows primary products for the $n=3$ cluster, but also primary product ions accompanied by loss of one or two solvent molecules. The fourth panel shows similar data at a lower photon energy, where less extensive fragmentation is observed.

Data like those shown in figure 4 are obtained over a range of photolysis wavelengths or energies. By summing daughter ion intensities and normalizing to residual parent ion intensity at each wavelength, these mass spectra yield total photodissociation spectra and branching ratio measurements. In the next section a number of such datasets will be presented. In addition, a careful analysis of the fluence dependences for production of the combination channels demonstrates that they are the result of sequential absorption of photons. This analysis will provide clear mechanistic insight into the dynamics of the photodissociation process.

5. Size-dependent photodissociation spectra

Photodissociation spectra are available for several systems in which the alkaline earth cations Mg^+, Ca^+, or Sr^+ are bound to polar solvents such as NH_3, H_2O, CH_3OH, and CH_3NH_2 and selected isotopomers of these species. In the next sections we will present representative sets of experimental results, illustrating consistent trends in the evolution of electronic states as a function of cluster size, and the variation of product branching ratios vs. size and wavelength. We will also comment on the selectivity of reactions via photoexcitation as compared with metastable decay from internally excited parent ions, and the structures and reactivities of unusual species incorporating distinct chromophores within the same cluster.

5.1. $Sr^+(CH_3OD)_n$

This system has been the subject of extensive investigation [24, 27, 28], both in terms of the evolution of the total photodissociation signal vs. cluster size and product branching ratios. The primary single-photon dissociation reactions are given by equations (2)–(4):

$$Sr^+(CH_3OD)_n \rightarrow Sr^+(CH_3OD)_{n-1} + CH_3OD \quad (2)$$

$$\rightarrow SrOD^+(CH_3OD)_{n-1} + CH_3 \quad (3)$$

$$\rightarrow SrOCH_3^+(CH_3OD)_{n-1} + D \quad (4)$$

Figure 5 shows a schematic reaction coordinate for these primary photoproducts in the specific case of the monomer, $n=1$. The diagram shows that solvent evaporation, –L, is a simple bond cleavage process, endothermic by 23 kcal mol^{-1}. Both the –Me and –D channels are reactions that result in oxidation of the metal ion, a process that is accompanied by simultaneous bond breaking and bond formation. Therefore, we expect both these channels to proceed over activation energy barriers in excess of the reaction endothermicity. The nature of these barriers is discussed below. Figure 6 shows a portion of the photodissociation spectrum for the monomer, obtained

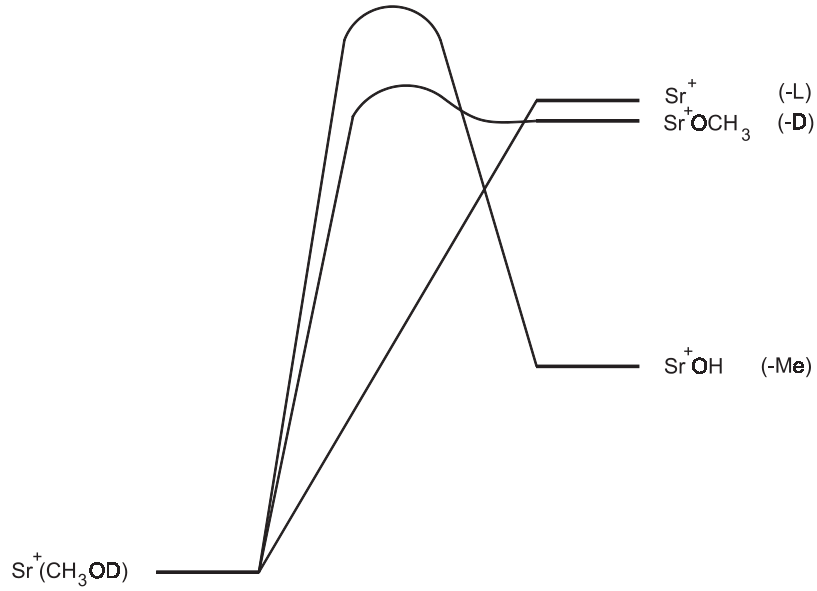

Figure 5. Reaction coordinate for formation of primary photoproducts in $Sr^{+}(CH_3OH)$.

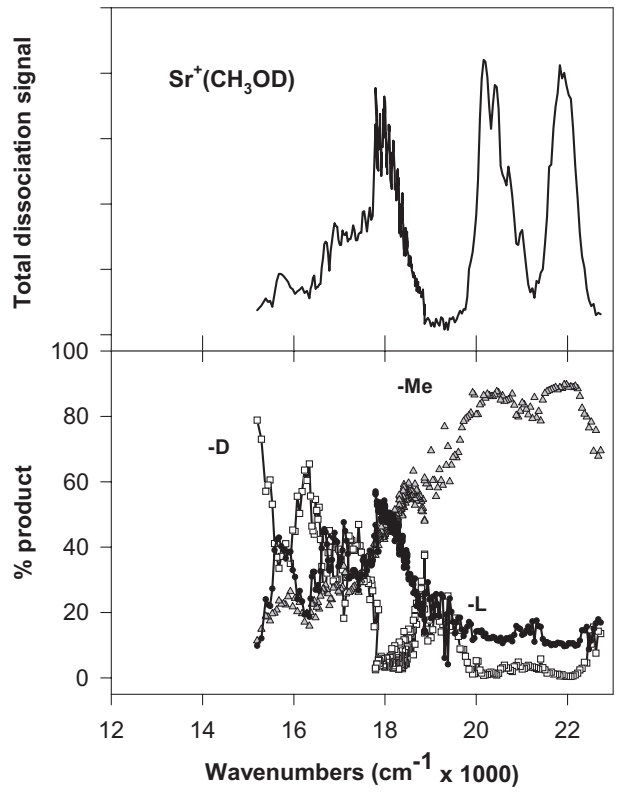

Figure 6. Top panel: photodissociation spectrum for $Sr^{+}(CH_3OD)$. Bottom panel: branching fractions for ligand loss (–L), methyl loss (–Me), and deuterium atom loss (–D). Figure reprinted from reference [28] with permission.

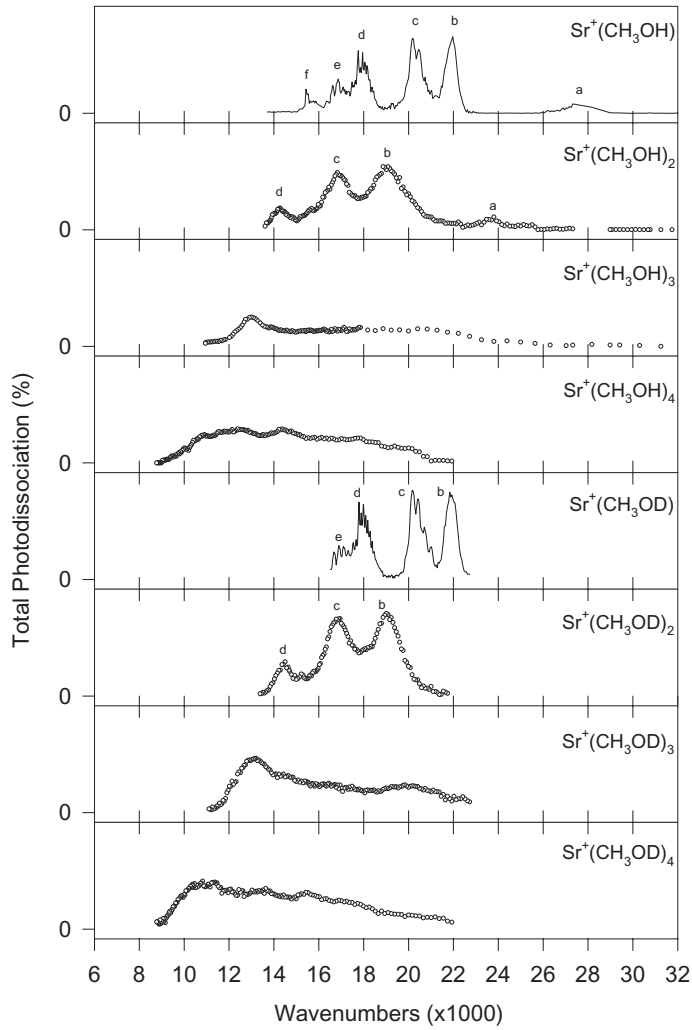

Figure 7. Photodissociation spectra of $Sr^+(CH_3OH)_n$. Monomer and dimer spectral maxima labelled with letters a–f which are assigned to transitions from the ground electronic state to the following states: a, $(6)^2A'$ (5pσ); b, $(3)^2A''$ (o-p 5pπ); c, $(5)^2A'$ (i-p 5pπ); d, $(4)^2A'$ (4dσ); e, $(2)^2A''$ (o-p 4dπ); f, $(3)^2A'$ (i-p 4dπ). Figure reprinted from reference [28] with permission.

with CH_3OD as the solvent. The lower panel of this figure shows the branching ratios for the –L, –Me, and –D channels, corresponding to reactions (2), (3) and (4) respectively.

In the upper panel of figure 7, we show the total dissociation signal over the full wavelength range for the monomer cluster, with CH_3OH as solvent. This cluster exhibits six resolved bands, ranging in energy from approximately 15000 to 27000 cm^{-1}, which we have assigned in a previous publication in analogy with *ab initio* calculations on the $Sr^+(H_2O)$ system [66]. The highest energy band in $Sr^+(CH_3OH)$, denoted 'a', is a transition to a 5pσ-like state; below that band, we find two well-resolved electronic bands, 'b' and 'c', assigned to 5pπ-like states. The bands that appear in the low energy portion of the monomer spectrum, 'd'–'f',

correspond to transitions that access states with 4d atomic character. The partially-resolved vibrational structure in the 4dσ and 4dπ bands has been discussed previously [24, 67].

The branching ratios for the primary photoproducts provide significant information about the nature of the excited states leading to those fragments. Both the dependences on cluster size and on the level of internal excitation of the precursor parent provide important insight into the barriers on the potential energy surfaces and the manner in which parent ion internal energy helps surmount those barriers. The branching ratios for photolysis products from the monomer produced directly from the supersonic expansion source, shown in the lower panel of figure 6, provide an important baseline for that discussion. At the longest photolysis wavelengths, the –D channel competes favourably with the simple –L channel, as expected from the comparable endoergicities for each channel. Surprisingly, the least endoergic channel, –Me, is nearly absent at the very red end of the spectrum and does not become a dominant channel until the much higher energy 5pπ bands are accessed. The data suggest that the barrier for methyl loss is higher than that for D loss.

Crossed molecular beam work by Davis *et al.* [68] on the related $Ba + CH_3OH$ system provides insight into the issue of the relative barrier heights. These experiments showed that both ground (^1S) and excited (^1D) Ba electronic states formed the $BaOCH_3$ product by H-atom loss almost exclusively, despite the fact that the BaOH channel is less endoergic. This selectivity was explained in terms of a facile hydrogen atom migration process aided by the spherical symmetry of the 1s orbital of H, which allows simultaneous overlap with both the metal and the oxygen atom on CH_3OH. In contrast, the elimination of a methyl radical is expected to proceed only when the $O–CH_3$ bond is nearly broken, suggesting a substantial potential energy barrier to this reaction. Two key *ab initio* calculations on related systems support this picture: transition metal catalyst activation of H–H and $H–CH_3$ bonds show that the H–H bond is facile to activate, while insertion to form an $H–M–CH_3$ intermediate occurs only over a substantial potential energy barrier [69, 70]. The work of Sulzbach *et al.* [71] on hydrogen atom and methyl radical migration in dialkyl carbenes also supports the claim that the barrier for methyl migration is considerably higher than that for H migration.

The notion that the barrier for the –D channel is lower than that for the –Me channel is consistent with our experimental observations. All channels are energetically accessible throughout the photon energy range of these experiments, but at lower photon energies, the less restricted transition states for the –D and –L channels dominate the dissociation kinetics. The data support the idea that the –D channel proceeds through a migration process over a barrier lower than that of the insertion process leading to methyl loss. Therefore, at low photolysis energies, the –D channel and the solvent evaporation channel, which we expect to occur without a barrier in excess of the endoergicity, dominate over –Me. However, well above the threshold for the –Me channel, the constraints of the higher barrier are much less restrictive, and that product becomes strongly favoured, as is shown in the branching ratio data for the 5pπ bands.

The –D loss channel is only accessed in the lowest energy portion of the spectrum, and competes very effectively with the ligand loss channel in this wavelength regime. The simple evaporation of solvent occurs directly, without overcoming a potential energy barrier, and therefore one might expect the –D channel to be a

minor process in this portion of the spectrum. The transitions to low-lying d orbitals of Sr^+ are excited in this region of the spectra. As Sanekata *et al.* proposed in their work on the $Ca^+(H_2O)_n$ system, the proximity of the ^2D-derived states to the ground electronic state may facilitate internal conversion (IC) and allow more facile elimination of a deuterium atom relative to the higher-lying states of ^2P character [72]. This issue may be an important factor in $Sr^+(CH_3OD)_n$ as well, and leads to the effective competition of the –D channel with –L throughout the electronic bands based on Sr^+ 4d-orbitals in the low photolysis energy regions of the spectra. This situation contrasts with the $Mg^+(CH_3OD)$ system [26], in which –Me is the exclusive product over the entire wavelength range, indicative of facile selective overlap of the metal p-orbital with the C–O σ^* antibonding orbital. Thus, the differences in reactivity between the Mg^+ and Sr^+ species are direct manifestations of differences in electronic structure of the metal ions.

The total dissociation spectra for forming all product channels as a function of cluster size are plotted in figure 7. 'Product switching', which makes the $Sr^+(CH_2OD)(CH_3OD)_n$ cluster the dominant species in the parent mass spectrum for $n \geq 3$, limits the range of Sr^+-based clusters that our experiments can probe. The spectra show broadening and red shifts that increase with cluster size. The broadening occurs in large part because of inefficient cooling of the larger clusters. These clusters are probably created by larger precursors that have undergone solvent evaporation, and therefore retain significant internal excitation. The density of accessible states increases with increasing cluster size, so spectral congestion also contributes to the broadening. The existence of conformational isomers may also cause inhomogeneous broadening in the spectra.

The large red shifts that occur with increasing cluster size are clearly the most salient features in the size-dependent spectra. The experimental data for numerous other systems with similar 'core' electronic structure studied in our group and by others show qualitatively similar behaviour. In broad terms, the size-dependent red shifts provide information on the modification of atomic ion transitions as a function of the solvation environment. Both solvent shell closing effects and properties that reveal information on the 'diffuseness' or ion-pair character of ground and excited electronic states come into play. We will therefore defer discussion of the electronic structure issues that this class of clusters raises until we have presented experimental data for a range of systems and have called attention to the unifying characteristics of these data.

5.2. $Mg^+(CH_3OD)_n$

The dissociation spectra for this system [26] share many features with the related $Sr^+(CH_3OD)_n$ studies. Vibrationally-resolved photodissociation spectra on the singly-solvated cluster ion have been reported by Duncan and co-workers [73]; however, photodissociation measurements on the larger clusters were reported only at selected wavelengths. Stepwise binding energies in the $Mg^+(CH_3OH)_n$ system have been measured in collision-induced dissociation experiments reported by Armentrout and co-workers [23]. Stace and co-workers [74] have examined the mass spectra of clusters based on Mg^+ and Mg^{2+} bound to methanol and have found that the singly-charged metal ion clusters show significant product switching via H atom ejection when $n \geq 3$. In our laboratory, careful control of ion source conditions produces clusters with stoichiometry $Mg^+(CH_3OD)_n$, for $n = 1$ to 5, allowing complete dissociation spectra and product branching ratios to be measured. A small

amount of product switching in the ground states of parent ions is attributed to C–H bond cleavage, a fact consistent with the results reported by Woodward *et al.* [74]. The electronic transitions observed in these clusters are based on excitations from the cluster ground states, in which the Mg^+ ion has strong ^2S character, to excited states with ^2P character. The spectra exhibit strong red shifts as the second and third solvent molecules are added, but the addition of a fourth or a fifth solvent molecules result in very small red shifts. This observation is consistent with the closure of the first solvent shell with three solvent molecules, as observed by Fuke and co-workers in the $Mg^+(H_2O)_n$ system [75].

The singly-solvated $Mg^+(CH_3OD)$ cluster shows strong selectivity in photochemical product formation, undergoing methyl loss exclusively to form $MgOD^+$, despite the fact that the evaporation process has a lower barrier. This observation suggests that the details of the non-adiabatic interactions between the excited and ground states are of critical importance. Methyl loss continues to be a major product channel for the first three clusters, but is not observed in the fourth and fifth clusters. The significant barrier for C–O bond cleavage allows this channel to be competitive in the first solvation shell, but the much weaker electrostatic forces between solvent molecules in the second shell provide low energy channels that make solvent evaporation the dominant process for the largest clusters.

Selective photochemical cleavage of O–D bonds becomes an important reactive channel in the largest clusters, but only when the ejected D atom is accompanied by a solvent molecule. This observation has particularly interesting consequences for the $n = 2$ cluster, in which the –Me and –L channels are observed as in the monomer; D-loss is also observed, but only in the form of the combination channels –(Me + D), and –(L + D). These latter channels are dominant at the shortest photolysis wavelengths. The similarity of the product distributions in this wavelength range leads us to suspect that the deuterium atom loss occurs by a similar mechanism in both these channels. In the –(L + D) channel, the deuterium atom clearly must come from a ligand other than the one lost by evaporation. As its wavelength dependence is similar, it is possible that the deuterium atom from the –(Me + D) channel may also be taken from the other ligand. The product from such a reaction mechanism is a methoxy/hydroxy solvated cation of the form H_3COMg^+OD, while a ligand solvated monoxide H_3CODMg^+O is produced by elimination of both Me and D from the same ligand. Thermochemical estimates suggest the minimum endothermicities for production of H_3COMg^+OD and H_3CODMg^+O at 10 and 40 kcal mol^{-1}, respectively [26]. The energetics suggest that the production of H_3COMg^+OD via the double ligand cleavage mechanism is much more favourable.

This piece of evidence on the methyl fragment and deuterium atom being lost from different ligands helps to understand why the –(Me + D) channel occurs only in the dimer. The dimer must have a unique structural element that allows the reaction to take place. The lowest potential energy dimer structure calculated by Lu and Yang [30] shows that the methyl group of one ligand is placed in close proximity to the deuterium atom of the other ligand. Once a methyl radical is created by C–O bond cleavage, it is in an ideal position to abstract a deuterium atom to create CH_3D. This geometry, which allows facile production of CH_3D, is not found in the larger cluster structures. This concerted mechanism for the elimination of methane is similar to that proposed by Davis *et al.* in their work on collisions of $Ba + CH_3OH$ [68].

5.3. $Sr^+(NH_3/ND_3)_n$

The $Sr^+(NH_3/ND_3)_n$ systems are among the first ones probed in our laboratory [53, 54, 76, 77] and have provided a number of interesting avenues for research. Clusters in which parent ions are formed by simple electrostatic binding of metal to solvent are particularly easy to form, since there are no chemical reactions that may oxidize the metal or cleave covalent bonds in the solvent. As we have noted earlier, typical operating conditions for laser vaporization production of clusters yield mass spectra with local intensity maxima and minima. The first group of cluster ions has an intensity distribution that peaks near six solvent molecules and goes through a local minimum around 10 to 11 solvents [63]. Photolysis of these clusters occurs exclusively by evaporation of solvent molecules. Thus, the $Sr^+(NH_3/ND_3)_n$ system provides an example of one in which oxidation of the metal ion does not appear to be a significant reaction channel either in the ground state or in excited electronic states.

The photodissociation spectra for the first nine cluster ions are shown in figure 8. Assignments for the first three clusters are aided by *ab initio* calculations reported by Bauschlicher, Sodupe and Partridge (BSP) [66]. The singly-solvated cluster shows two bands: the lower-energy feature at 17300 cm^{-1} is assigned to the (2) $^2A_1(4d\sigma) \leftarrow (1)\ ^2A_1(5s)$ transition. *Ab initio* calculations place this transition at 17700 cm^{-1}, and show that 5p/4d orbital coefficients are in the ratio of 0.43/0.59. The higher energy feature at 20450 cm^{-1} is a spin–orbit doublet. The low-energy band of the doublet at approximately 20240 cm^{-1} is assigned to the (3) $^2E_{1/2}(5p\pi) \leftarrow (1)\ ^2A_1(5s)$ transition, while the high-energy band at 20660 cm^{-1} is assigned to the (3) $^2E_{3/2}(5p\pi) \leftarrow (1)\ ^2A_1(5s)$ transition. Both of these bands exhibit vibrational sequences in the Sr–N stretching mode. The measured vibrational spacing of 210 cm^{-1} in the (2) $^2A_1$ state of $Sr^+(NH_3)$ agrees quite well with the *ab initio* prediction of 214 cm^{-1}. The higher energy band has a vibrational spacing of 290 cm^{-1}, again in good agreement with the value calculated for the Sr^+–NH_3 stretch, 272 cm^{-1}. The magnitude of the splitting in this band is 420 cm^{-1}, intermediate between the spin–orbit interaction of the $^2D_{5/2-3/2}$ (280 cm^{-1}) and the $^2P_{3/2-1/2}$ (801 cm^{-1}) states of the bare ion, Sr^+. This observation implies that the $^2E_{3/2-1/2}$ state of the complex is formed from a linear combination of 4d and 5p atomic orbitals [78]; the BSP calculations show that the orbital coefficients for those states are 0.14 and 0.82 respectively.

$Sr^+(NH_3)_2$ has two distinct electronic transitions: the first one occurs at 17300 cm^{-1}, with a higher-energy band at 22200 cm^{-1}. In agreement with earlier work from this laboratory [77] the dimer complexes are predicted by BSP to have a linear D_{3d} symmetry, as a result of sdσ hybridization of the ground state. We assign the band at 17300 cm^{-1} to the (1) $^2E_u(5p\pi) \leftarrow (1)\ ^2A_{1g}(5s)$ transition. The measured frequency differs only by 1000 cm^{-1} from the BSP calculations. This band displays a partially resolved splitting of 390 cm^{-1}, which we attribute to a spin–orbit interaction. The higher-energy band at 22200 cm^{-1} is assigned to the (1) $^2A_{2u} \leftarrow (1)\ ^2A_{1g}(5s)$ transition and can be compared to the calculated value of 25700 cm^{-1}. Both of these transitions are to states with a high degree of 5p state character.

The trimer of the strontium–ammonia system is predicted by BSP to have a 'T-like' structure. We observe at least three distinct transitions for these complexes. The most intense bands at 13300 cm^{-1} are assigned to the (2) $^2A' \leftarrow (1)\ ^2A'$ transition, with 5p/4d mixing in the ratio 0.80/0.32 and agreeing quite well with the calculated value of 14000 cm^{-1} from BSP. The remaining transitions shown in

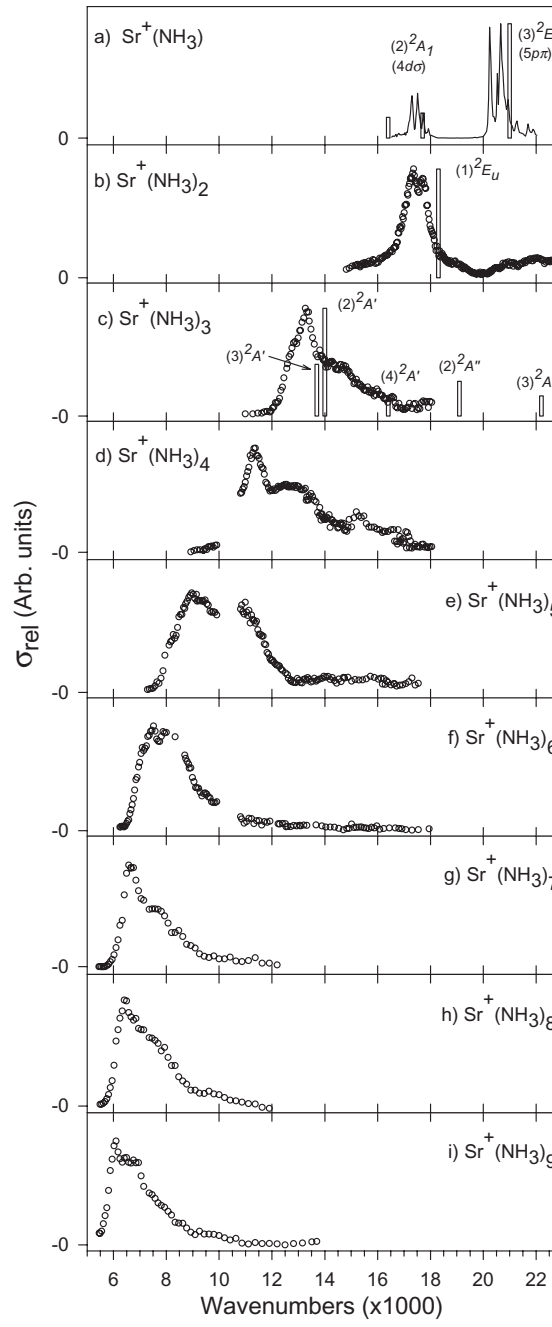

Figure 8. Photodissociation spectra of $Sr^+(NH_3)_n$, $n = 1$–9. Electronic states and intensities from the calculations of reference [66].

figure 8 are to final states with significant 5d/4p mixing: the (3) $^2A'$ and (4) $^2A'$ states have 5p/4d mixing ratios of 0.50/0.62 and 0.26/0.90 respectively.

The complexity of the $Sr^+(NH_3)_n$ systems has hindered *ab initio* calculations for clusters with more than three solvent molecules. Population analysis of the electronic

states in these systems demonstrates that the transitions in these clusters occur between states that have strong atomic ion parentage. Although the calculations have been limited to three solvent molecules, the work suggests that increasing metal–ligand repulsion in the series $Sr^+(NH_3)_n$, with $n=1$ to 3, raises the ground state energies of $Sr^+(NH_3)_n$ relative to their excited states. In conjunction with stronger mixing of cluster ion states that correlate with ^2P or ^2D atomic ion states in $Sr^+(NH_3)_3$, the net effect of the increased repulsion is to generate cluster ion states with excitations below $14000\,cm^{-1}$ that carry significant oscillator strength. Such a prediction is consistent with the fact that the absorption spectrum for $Sr^+(NH_3)_3$ shows a significant red shift relative to smaller clusters.

The photodissociation spectra of figure 8 show that the red shift continues to increase with increasing cluster size up to six solvent molecules. Clusters with 7, 8, or 9 solvent molecules have dissociation spectra that resemble that of the $n=6$ species, the additional solvent molecules providing slight perturbations on the basic form of the $n=6$ spectrum. It is reasonable to expect that interactions of the solvent lone-pair electrons with the metal valence electron should be maximized for molecules in the first solvation shell. As these interactions result in red shifting of the spectrometric signals, the spectra for larger clusters are consistent with a closed first solvent shell structure at $n=6$.

The large size-dependent red shifts observed in the $Sr^+(NH_3)_n$ were first reported by Shen *et al.* [79]. Because the spectra appeared to evolve toward the shape of the spectrum of metal–ammonia solutions [80], a thermodynamic argument that estimated the energies of charge-transfer states of the form $Sr^{2+}(NH_3)_{n-m}(NH_3)_m^-$ was employed. It suggested that the decreasing energy gap between the ground state of the cluster and these charge transfer states might account for the size-dependent spectral behaviour. The possibility of strong ligand field-induced mixing [78] of the 4d atomic orbitals of Sr^+, which lie $9616\,cm^{-1}$ below the 5p orbitals, into the excited states of the clusters, cast doubt on this interpretation [66]. However, experimental data on systems to be discussed in later sections in which the lowest-lying d orbitals lie significantly *above* the p orbitals, i.e. systems based on Li, Na, Mg^+, are not affected by this ligand field mixing. The data thus provide an additional point of comparison in establishing patterns in the size-dependent spectra of such systems.

5.4. *Hydrates of Mg^+, Ca^+ and Sr^+*

The spectroscopy of one-electron chromophores like alkali metals or singly-charged alkaline earth cations bound to polar solvent molecules raises the important issue of how the electronic structure of such clusters evolves from that of the core atom to metal-centred states in small aggregates, to the bulk, solvated electron state. The cluster ions formed by hydration of the singly-charged alkaline earth cations Mg^+, Ca^+ and Sr^+ provide a critical case study by allowing systematic variation of the atomic ion ^2S–^2P energy gaps, the binding energies of solvent molecules to ions, the second ionization potential (IP) of the metal, and the role of low-lying ^2D states that contribute to allowed electronic transitions via ligand-field mixing.

These metal ion–solvent systems present additional challenges relative to the Sr^+–ammonia system because of the possibility of metal atom oxidation reactions that occur during the cluster formation process. In their studies of the $Mg^+(H_2O)_n$ [31, 32] and $Ca^+(H_2O)_n$ systems, Fuke and co-workers [81–83] noted that parent

ions undergo 'product switching' in the size range from approximately 5 to 15 solvent molecules, where metal atom oxidation is driven by the formation of clusters based on $MgOH^+$ or $CaOH^+$ core ions. The first product switch occurs when the energy of the solvated MOH^+ moiety falls below that of solvated M^+. Although the reactant ions switch back to favour solvated M^+ at approximately 15 solvent molecules, the reasons for this change are unclear; one possible reason advanced for this second switch is spontaneous ionization, in which intracluster electron transfer to forms species with a two-centre charge distribution. Hydrates of Mg^+ can be made with up to five solvent molecules, while Ca^+ hydrates can be formed with up to six solvent molecules. The reactions that lead to the first product switch to produce solvated MOH^+ species have an H/D isotope effect that allows some control over the ratio of clusters based on M^+ or MOH^+. In the $Sr^+(H_2O/D_2O)_n$ system, the cluster distribution can be manipulated to favour cluster ions with the Sr^+ core out to $n=6$ by employing D_2O vapour in the ion source [25].

Figure 9 shows the photodissociation spectra for $Sr^+(D_2O)_n$, with $n=1$ to 6 taken with the Rochester instrument [25]. Aside from the smaller range of clusters that can be produced in this system because of product switching, the size-dependence of the spectra resembles that observed for the Sr^+–ammonia system. The singly-solvated cluster shows three absorptions corresponding to excitation of the (2) $^2B_2$, (2) $^2B_1$, and (4) $^2A_1$ states formed from the 5pπ (in-plane), 5pπ (out-of-plane), and 5pσ atomic ion orbitals respectively, and a single absorption band to the (3)$^2A_1$ (4dσ) state. The branching fractions for dissociation products strongly favour the oxidation process to form $SrOH(D)^+$ reaction products. The lack of any significant electronic state dependence with the branching fraction is consistent with a dissociation mechanism in which the excited state undergoes rapid internal conversion (IC) to the ground state.

The spectrum for the doubly-solvated ion is broadened and red-shifted relative to the monomer, and the band intensities and positions are in reasonably good agreement with *ab initio* calculations [66]. Clusters with two or more solvents illustrate a reactivity pattern that holds for the higher clusters: at low photolysis frequencies, where the accessible electronic states have significant ^2D atomic ion parentage, the oxidation products are favoured, presumably because the low-lying ^2D states facilitate internal conversion and subsequent O–D bond activation [72]. The higher energy states favour solvent evaporation.

The trimer spectrum shown in figure 9 is a red-shifted and broadened version of the dimer spectrum, with general spectral positions and intensities in agreement with *ab initio* band origin calculations. The general trends in the dissociation spectra for the $n=4$, 5, and 6 clusters are similar to those observed in the analogous ammonia system. The spectrum rises rapidly at the red end and tails to higher frequencies. The *ab initio* calculations of BSP show that the ligand–field interactions in the trimer cause the ordering of the molecular electronic states to be different from those in the bare atomic ion. In the monomer and dimer, the lowest energy cluster states are predominately 4d in character, reflecting the low-lying nature of the 4d atomic ion states relative to the 5p states. However, in the trimer, the calculations of BSP show that the lowest energy transition is predominately 5p in character, giving that transition the largest oscillator strength in the manifold of excited states. This low-lying (1) $^2B_1$ state is formed from 5p orbitals that have π-type interactions with the lone pair electrons of the solvent. All remaining orbitals with 4d or 5p character have σ-type interactions with the solvent molecules in the T-shaped trimer,

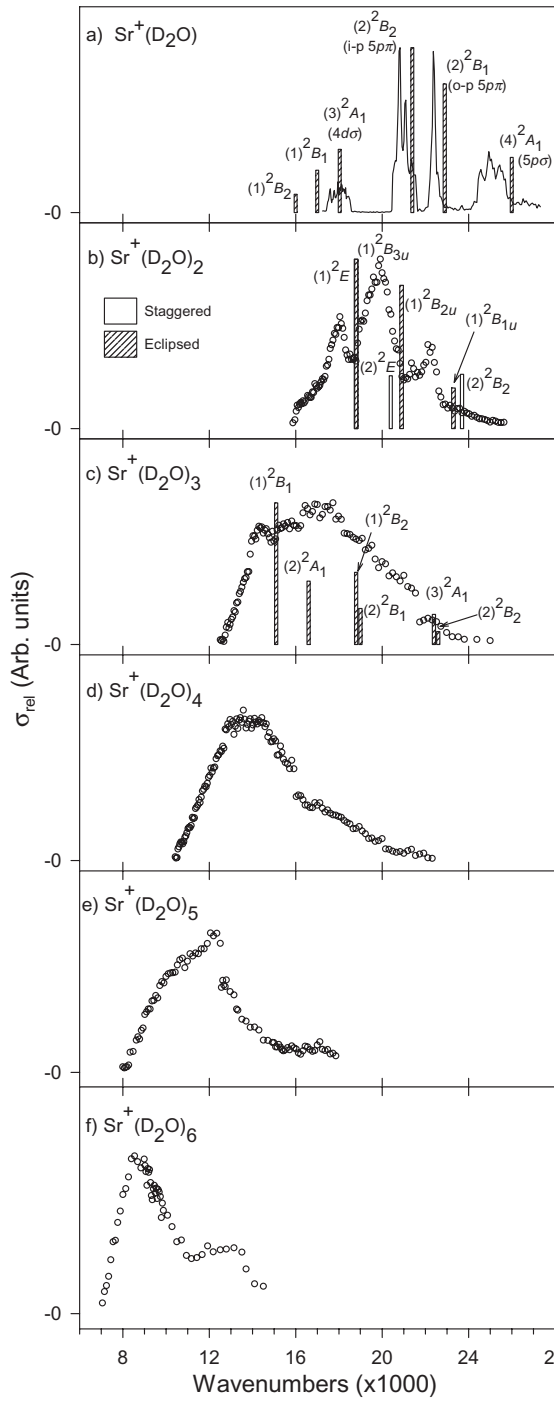

Figure 9. Total photodissociation signals for $Sr^{+}(D_2O)_n$, $n = 1$–6. Each data point corresponds to a wavelength at which dissociation data was obtained. To clarify the details of the monomer spectrum, a continuous line connecting all data points is substituted for the individual symbols. Calculated transition frequencies and strengths from BSP are indicated as superimposed bar plots. The symmetry labels correspond to the calculated states. Figure reprinted from reference [25] with permission.

raising their energies. The fact that the larger clusters have this same spectral feature suggests that the state re-ordering mechanism that generates a low energy state with significant 5p character is operative in the larger clusters. The spectrum of the $n=6$ cluster has a shape very similar to that of the corresponding ammonia-based cluster. The spectra also appear to narrow in that same size range. An extension of the ideas advanced in the work of BSP for the smaller clusters indicates that the size-dependent red shift may have its origins in metal–ligand repulsions that increase in magnitude as the first solvation shell is filled.

The spectra of hydrates of Mg^+ provide interesting counterpoints to the results for the Sr^+-based systems. Strong product switching only allows the spectra of the $n=1$ to 5 species to be determined [31, 32]. A high-resolution version of the spectrum of the singly-solvated species has been reported by Duncan and co-workers [84, 85]. The results reported by Fuke and co-workers [32, 86] without vibrational resolution are shown in figure 10. The spectra are remarkably similar in form to those of the Sr^+-based system in that the second and third solvent molecules induce strong red shifts relative to the absorption positions of the monomer. The small perturbations in the spectra for $n=4$ and 5 relative to the $n=3$ species are consistent with filling of the first solvent shell at $n=3$. *Ab initio* calculations appear to predict correctly the positions of the excited states in the small clusters [32, 66, 87].

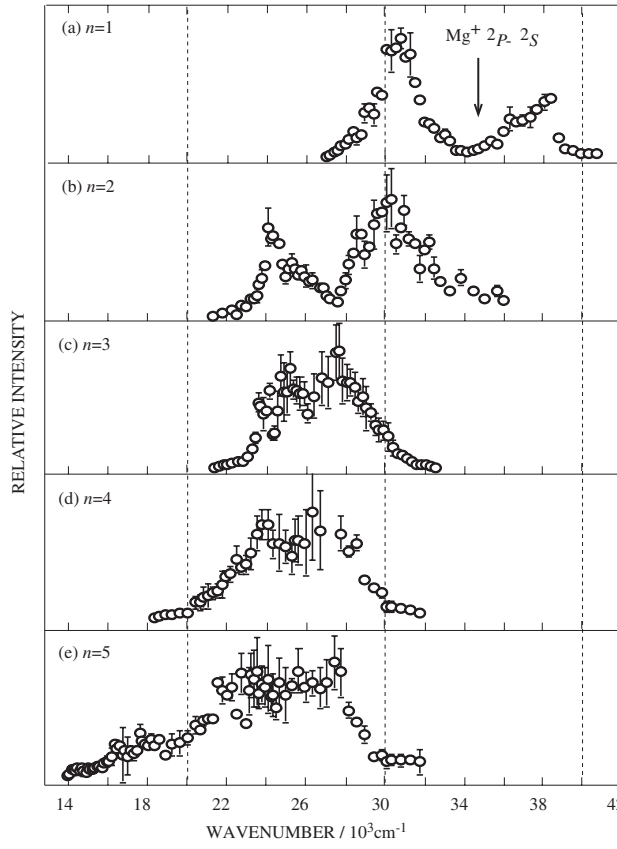

Figure 10. Total photodissociation signals for $Mg^+(H_2O)_n$, $n=1$–5 in panels (a) through (e) respectively. Figure reprinted from reference [75] with permission.

Calculations also suggest that the origin of the size-dependent red shift is metal–ligand repulsion, and that the presence of several isomeric structures for the $n=4$ and 5 clusters accounts for the shading of the spectra toward the red for the last two clusters [88, 89].

The product distributions are of particular interest in this system. For the $n=1$ cluster, the $MgOH^+$ product accounts for over 80% of reaction products, independent of photolysis wavelength. This observation suggests that photoexcitation is followed by rapid internal conversion to the ground state, where dehydrogenation occurs with metal oxidation. In contrast, the $n=2$ and 3 clusters exhibit a strong wavelength dependence and $MgOH^+$ formation appears to be enhanced above $28600\,cm^{-1}$, where the in-plane (2) $^2B_2$ excited state becomes accessible. The intracluster reaction in the $n=4$ and 5 clusters does not show a wavelength dependence consistent with excited state reaction; this suppression may be caused by the additional internal degrees of freedom of second solvation shell molecules, which facilitate rapid internal conversion to the ground state surface.

The spectra of figure 10 show the same size-dependent patterns as the previous systems we have discussed. The spectral red shifts in the first solvation shell are substantial, but the addition of a fourth or fifth solvent molecule results in very small additional shifts. Theoretical work by Watanabe and Iwata [88] suggests that metal–ligand repulsion accounts for the red shift in the first shell. The fact that the low energy limit in these systems occurs significantly to the blue relative to the corresponding Sr^+ systems correlates with absence of low-lying ^2D states that may participate in ligand–field state mixing.

As a final point of comparison, figure 11 shows the results of photodissociation experiments on the $Ca^+(H_2O)_n$ system [72]. This system behaves very much like the Sr^+-based clusters, both in terms of the familiar size-dependent spectral motif and the fact that the first solvation shell appears to fill with six solvent molecules. As in the Sr^+ hydrates, the presence of low-lying 3d orbitals appears to generate low-lying states that lead to strong red shifting and to enhanced dehydrogenation at low photon energies. Fuke and collaborators [33, 89] comment that charge transfer states are not required to understand the spectral shifts in these systems, a point that is supported by *ab initio* calculations [90].

Despite the significant differences in electronic structure among the ions Mg^+, Ca^+, and Sr^+, experimental and theoretical work on the cluster hydrates suggests a number of unifying concepts. Dehydrogenation both in the ground and electronically excited states of these species is a facile process. The presence of low-lying ^2D states in the two heavier systems differentiates their low energy reactivity patterns, and to a significant extent, the long wavelength limit at which clusters with a filled first solvation shell absorb light and dissociate. However, more recent work on the related $Mg^+(NH_3)_n$ system [64, 65, 88, 89, 91], and new theoretical studies that probe valence electron distributions in $Mg^+(H_2O)_n$ [92–94], suggest that the preceding rather clean picture of electronic states and reactivities breaks down, and that a picture incorporating charge transfer states and electron transfer may indeed be a more correct description.

5.5. *$Mg^+(NH_3)_n$ and isoelectronic analogues*

The $Mg^+(NH_3)_n$ system is one that has received significant experimental and theoretical attention [91]. Of special note is the fact that the isoelectronic analogues $Na(NH_3)_n$ and $NH_4(NH_3)_n$ have also been studied with a variety of experimental

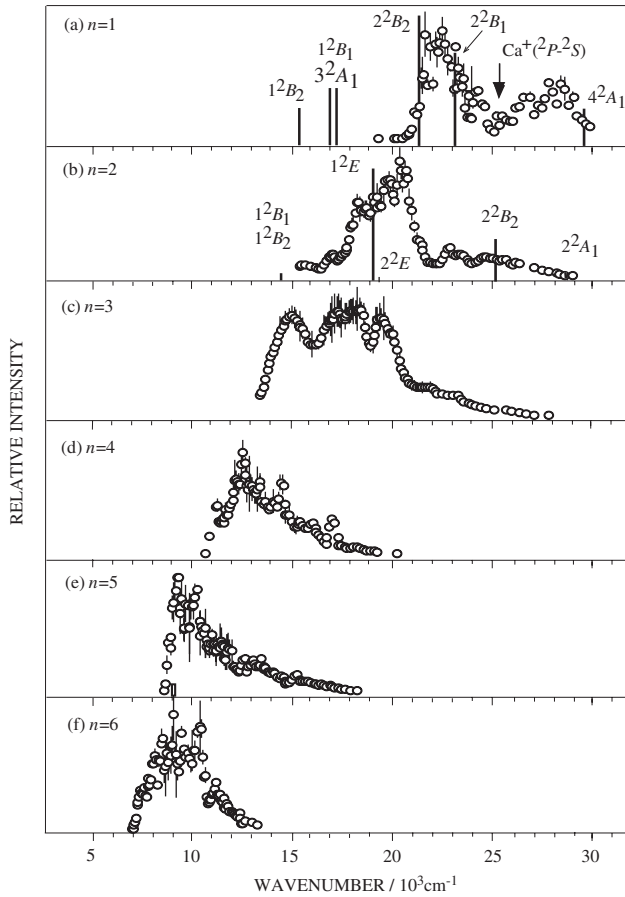

Figure 11. Total photodissociation signals for $Ca^+(H_2O)_n$, $n = 1$–6 in panels (a) through (f) respectively. Figure reprinted from reference [72] with permission.

and theoretical probes, and the consistency of the picture that has emerged concerning size-dependent aspects of the electronic structure of these species is striking. These systems differ considerably in the nature of their cluster cores, which are ionic, atomic, or polyatomic in the case of the Rydberg molecule. Nevertheless, the fact is that the spectroscopic motifs of these systems are remarkably similar, and this suggests that an understanding of the physics common to these systems is emerging.

Mass spectrometric collision-induced dissociation and reactivity studies have been reported for this system [23, 95–97]. Photodissociation results on this system have been reported by Fuke and collaborators [64, 65] for one to four solvent molecules. Supporting *ab initio* calculations [23, 65] on this system address important issues of ground and excited electronic state energies and transition moments, providing excellent comparisons with experimental data. Data from our own group [91] are in excellent agreement with those already reported, and extend up to seven solvent molecules. Those results are shown in figure 12.

The spectrum for the singly-solvated cluster shows a vibrationally-resolved band near 35000 cm^{-1} and a much weaker, featureless absorption near 28000 cm^{-1}.

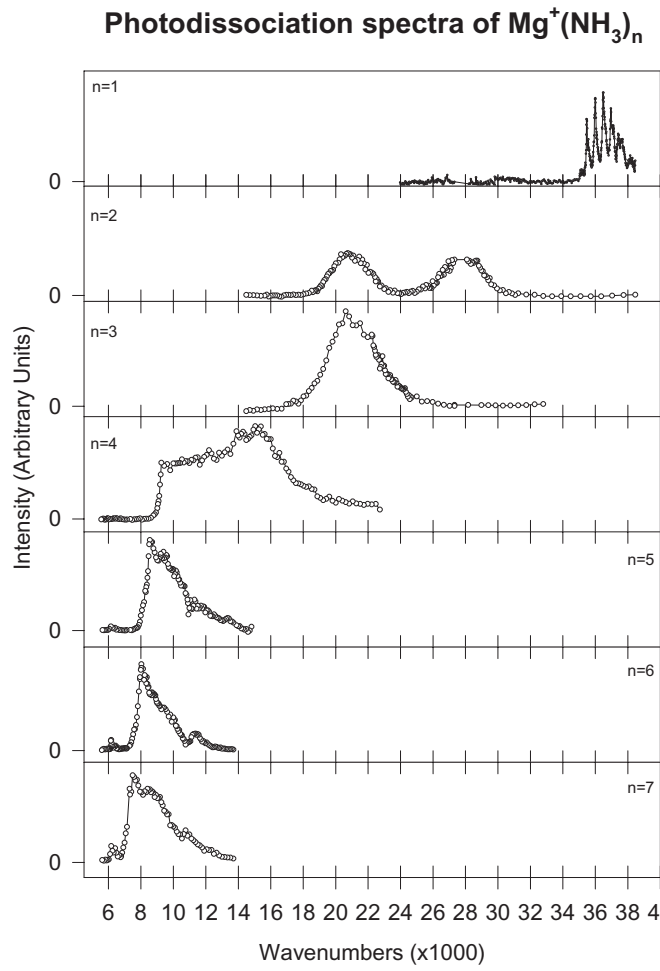

Figure 12. Total photodissociation signals for $Mg^+(NH_3)_n$, $n = 1$–7.

The higher energy feature corresponds to excitation of a $^2A_1$ electronic state in which the $3p_z$ orbital of Mg^+ points along the C_{3v} bonding axis. The weaker feature at lower energy corresponds to excitation to the ^2E state formed by the $3p\pi$ orbital set of Mg^+. The excited states accessed by the doubly-solvated $n = 2$ cluster can be assigned with assistance from *ab initio* calculations [65]. The ground state geometry of the cluster ion is bent, arising from $sp\sigma$ hybridization of the metal atom, and both excited states in this C_2-symmetric system are B_2 species that arise from the 3p orbitals on Mg^+. The red shifts relative to the monomer absorptions arise from metal–ligand repulsion. The trimer has C_3 symmetry, and the spectrum shows a strong peak near 21000 cm^{-1} with a much weaker peak near 22000 to 23000 cm^{-1}. The *ab initio* calculations help us assign the lower energy transition to excitation of a ^2E state and the higher energy one to a ^2A state. The motif of increasing red shift with increasing cluster size appears to hold in these systems.

The spectrum for $n = 4$ is particularly interesting, in that its unusual shape suggests that different structural isomers may make contributions to its appearance. The *ab initio* calculations help us with this interpretation: the broad feature that

peaks near 14000 cm^{-1} can be attributed to electronic transitions of a molecule having C_{2v} symmetry, in which all four solvent molecules interact directly with the atomic ion cluster core. Calculations predict that the two strongest transitions occurring near 1.76 eV (14200 cm^{-1}) and 2.08 eV (16800 cm^{-1}) correspond to excitation of $^2B_1$ and $^2B_2$ states based on the 3p orbitals of Mg^+. These transitions appear to be overlapped, with the lower energy one contributing to the long wavelength tail of the primary transition. The most notable feature of the $n=4$ cluster, the sharply rising edge near 9000 cm^{-1}, also appears in the spectra of the next three clusters, where its inherent narrow width reveals itself. The *ab initio* calculations are again helpful here, predicting that a second isomer of tetrahedral symmetry has a single strongly-allowed transition near 8500 cm^{-1}. The prediction is in good agreement with the position of the threshold for the sharply-rising feature observed for the $n=4$ cluster.

The spectra for the pentamer, hexamer, and heptamer can be interpreted in light of the foregoing assignment. Each of those spectra shows that the lowest energy feature appears to be fairly narrow; a series of partially resolved shoulders and peaks occurring at higher photon energies cannot be assigned definitively, but is likely associated with other structural isomers. In a tetrahedral ligand field, the 3p orbitals of Mg^+ remain degenerate, leading to the narrow absorption observed. The fact that the general shapes of the spectra for the larger clusters strongly resemble that deduced for the lowest energy feature in the tetramer suggests that the first solvation shell fills in $Mg^+(NH_3)_4$, and that the tetrahedral geometry forms the most stable core on which to build the second solvation shell.

The general features of the $Mg^+(NH_3)_n$ system can be examined in light of two important isoelectronic analogues. The first of these is the $Na(NH_3)_n$ system, reported by Hertel and collaborators [98], in which complete absorption spectra have been obtained. These measurements are made by monitoring the intensity of a specific parent cluster via photoionization, while scanning a second laser that probes vibrational transitions in the parent; these latter transitions decrease the parent cluster signal and lead to the term 'photodepletion' spectroscopy. Figure 13 shows the absorption spectra for the first six clusters in this series, showing that the well-resolved line spectrum of the singly-solvated cluster rapidly red shifts and broadens as additional solvents are added.

The $n=3$ cluster shows two major features: the first is a relatively sharp band with a width of ~500 cm^{-1} centred at 6600 cm^{-1}. That feature is present in the spectra of the $n=4$ to 6 clusters and is attributed to an overtone transition of the solvent, an interpretation claimed to be supported by isotopic substitution. Its intensity is derived from the atomic transition. The broad feature centred near 8000 cm^{-1} in the $n=3$ cluster is attributed to absorption by the metal–solvent system. In the $n=4$ to 6 clusters, the analogous absorptions appear as shoulders on the low frequency side of the putative overtone transition. These absorptions in the $n=5$ and 6 clusters are viewed as originating from a core cluster with its first solvent shell filled with four NH_3 molecules, the fifth and sixth solvent molecules occupying a second solvation shell in which the inter-shell solvent interactions only weakly perturb the basic chromophore. The metal–solvent absorption decreases in width from ~1500 cm^{-1} in the $n=3$ cluster to 700–1000 cm^{-1} in the larger clusters.

The experimental data of figure 13 show obvious similarities, but also clear differences with the corresponding ionic system. The earliest theoretical treatments of the $Na(NH_3)_n$ system [99, 100] were mounted to help understand size-dependent

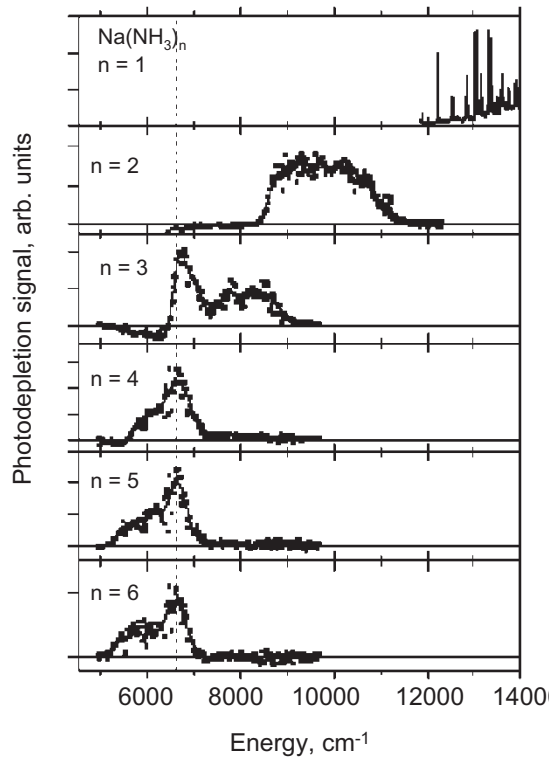

Figure 13. $Na(NH_3)_n$ depletion spectra for $n = 1$–6. Figure reprinted from reference [98] with permission.

ionization potential measurements, a topic we discuss in detail in section 7. For the present, we note that those calculations do provide some justification for thinking of the size-dependent red shifts as arising from increasing ion-pair character of the cluster ground states. More pertinent to the comparison between the neutral clusters based on the Na core and the ionic clusters built around Mg^+ is the idea that the most stable structures for the first four $Na(NH_3)_n$ clusters are interior structures that maximize the number of Na–N interactions [100]. In addition, only a single structure of D_{2d} symmetry is proposed for the lowest energy state of the tetramer. Such a structure provides a ligand field that partially lifts the degeneracy of the 3p orbital set on Na, and therefore does not predict a narrow low energy metal centred transition like that observed for the $n = 4$–7 $Mg^+(NH_3)_n$ clusters. However, the $Na(NH_3)_n$ clusters do exhibit a size-dependent red shift motif, in which large shifts occurring during the filling of the first solvation shell decrease significantly in magnitude, as the fifth and sixth solvents do not interact directly with the atomic core.

A final example of an isoelectronic system that shows the same spectroscopic signature as the preceding examples occurs in the very interesting series of clusters $NH_4(NH_3)_n$ based on the Rydberg molecule NH_4, which is isoelectronic with Na. The hypervalent ammonium radical has received much attention, and many experimental and theoretical probes of the structure and energetics exist in the literature. The absorption spectrum was first identified by Herzberg [101] and named after Schüler, who was among those who first observed it. The Schüler band of the

isolated ND_4 radical ($\sim$17200 cm^{-1}) has been assigned to the transition between the 3p $^2F_2$ state and 3s $^2A_1$ ground state [102]. The lifetime of the free radical was estimated to be less than 150 ns [103] while the fully deuterated analogue has a much longer lifetime > 10 μs [102–104]. It was recognized that the zero point energy difference between the very shallow potential wells of NH_4 and ND_4 is responsible for the large isotope effect. Ammoniation of the NH_4 radical has been shown to increase the metastable lifetime by several-fold [105, 106].

Clusters of radicals based on both isotopes were first identified by Gellene and Porter [103, 106, 107] in neutralization–reionization mass spectrometry, and more recent pioneering experiments by Fuke and co-workers have provided ionization potential measurements [108, 109] and complete absorption spectra for clusters with up to eight solvent molecules [110, 111]. The photoelectron spectroscopy experiments on the size-dependence of the ionization potentials of $NH_4(NH_3)_n$ clusters showed them to have a behaviour qualitatively similar to $Na(NH_3)_n$, and photodepletion spectroscopic measurements confirmed the similarities of the complete absorption spectra.

Figure 14 shows photodepletion spectra for the clusters $NH_4(NH_3)_n$, with $n =$ 1 to 8: the resemblance to the spectra of the isoelectronic species $Na(NH_3)_n$ and $Mg^+(NH_3)_n$ is striking. *Ab initio* calculations [111, 112] provide rigorous assignments that confirm the analogies in structures and spectra. Since NH_4 is equivalent to a sodium atom in the united atom limit, the molecular transitions of the cluster core can be referenced to atomic transitions. The singly-solvated cluster exhibits a sequence of vibrational bands beginning at 9305 cm^{-1} that are assigned to the (2) $^2A \leftarrow$ (1) ^2A transition originating from the 3p $^3F_2 \leftarrow$ 3s ^2A excitation in NH_4. The higher energy band with origin 10073 cm^{-1} corresponds to the (1) $^2E \leftarrow$ (1) ^2A transition. The transitions observed in the $n = 2$ to 4 clusters can be assigned to states that evolve from the 3p-based monomer transition. The spectral width of the band in the $n = 4$ cluster is at least a factor of two narrower than that of the preceding cluster, and reflects the fact that the tetrahedral geometry of the $n = 4$ ligand field allows all excited components of the 3p $^2F_2$ state to remain degenerate. Unlike $Mg^+(NH_3)_4$, in which the spectrum shows evidence for isomers of C_{2v} and T_d symmetry, the latter of lowest energy, the structure of the ammonium radical core provides a unique tetrahedral environment around which the ligands bind. The similarity of the spectra for the $n = 5$–8 clusters is consistent with the closing of the first solvation shell with four solvents and addition of the next four solvents to the second shell.

The similarities of the spectra for isoelectronic species $Mg^+(NH_3)_n$, $Na(NH_3)_n$ and $NH_4(NH_3)_n$ are no coincidence, and theoretical calculations suggest that two important factors are at work in establishing this common spectral motif: the first solvation shell fills in all three cases when four solvent molecules bind to the core; and, the electronic transitions are 3p $\leftarrow$ 3s in character. The strong red shift that occurs as the first solvation shell fills reflects the role that the solvent molecules play in driving the valence electron into a singly-occupied molecular orbital (SOMO) that is increasingly diffuse. We will build the case in the next sections that physics common to the spectra of these systems is also applicable to the other cluster systems in which alkaline earth cations are solvated by polar solvent molecules. To build this case, we will discuss the dynamics of the dissociation process and the evolution of the cluster electronic states with size. A complete understanding requires a close

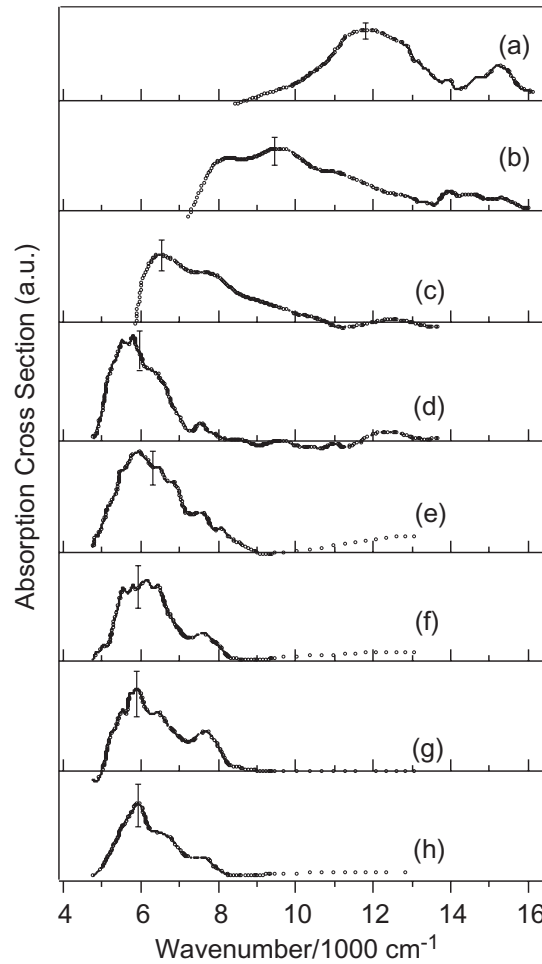

Figure 14. $NH_4(NH_3)_n$ photodissociation spectra for $n = 1$–8. Figure reprinted from reference [111] with permission.

connection between theory and experiment, and we will indicate areas where those connections can be strengthened.

6. Dissociation dynamics—electronic to vibrational energy transfer

The data presented in the previous sections provide examples of a number of distinct chemical phenomena including solvent evaporation, metal oxidation in the ground and excited electronic states, and reactions to form several competitive products. The photodissociation spectra also behave similarly with cluster size—namely, the red shift upon increasing solvation appears to reach near-saturation close to the filling of the first solvent shell. It is reasonable to ask what unifying electronic structure and dynamical concepts may help us understand the spectral and reactive similarities in these systems.

The electrostatic binding energies of polar solvent molecules to the open-shell alkaline earth ions are generally no more than 20 to 30 kcal mol^{-1}, and generally

decrease with increasing number of solvent molecules [23, 66, 113–117]. The lowest allowed electronic transition energies of the open-shell alkaline earth cations and the corresponding isoelectronic alkali metal atoms occur in the visible and near-UV regions of the spectrum. For example, in Sr^+, the $5^2S_{1/2} \leftarrow 5^2P_{1/2,3/2}$ transitions occur near 400 nm, and the corresponding transitions in Na occur at 589 nm. The energy gaps associated with these transitions correspond to 70 and 50 kcal mol^{-1} respectively, significantly in excess of the solvent bonding energies. Although the electronic states of clusters based on these transitions may be significantly shifted from their atomic ion parents, in general, one expects the electronic excitation energies of clusters to exceed the solvent binding energies. Clusters that absorb photons to such electronically excited states are metastable, and may thus decompose on a timescale appropriate to energy transfer processes that transform electronic excitation into vibrational (and translational) motion.

Because photodissociation events are often termed 'half-collisions', models of collisional quenching of electronically excited atoms provide guidance in interpreting the dissociation mechanism. One of the earliest descriptions of collisional quenching of electronically-excited alkali atoms, the Bauer–Fisher–Gilmore model [118], was based on the 'harpooning' mechanism employed to describe chemical reactions of alkali atoms with molecules [119, 120]. The model suggests that long-range electron transfer from the excited alkali M* to the molecular collision partner XY first forms a nascent M^+–XY ion pair. The collision system then evolves on the ion-pair surface, during which time the temporary molecular anion transfers its electron back to the alkali metal to form a ground state atom. The Franck–Condon factors for overlap of the XY^- vibrational wavefunctions with those of the neutral XY molecule at the instant of electron transfer determine the degree of vibrational excitation of the neutral product.

Although the Bauer–Fisher–Gilmore model is simplistic, it does provide a physical picture for electronic to vibrational energy transfer whose features are preserved in more sophisticated models such as the 'bond-stretching attraction' model advanced by Hertel and co-workers [121]. This model, which is similar in spirit to a model for collisional ionization developed by Los and collaborators [122], is based on surface crossings of ground and excited potential energy surfaces that occur in distorted molecular geometries. For example, the potential energy surface for the approach of Na* (^2P) to H_2 in C_{2v} symmetry does not exhibit a crossing with the ground state surface for H_2 in its equilibrium configuration. When the H_2 bond is extended, however, the excited state potential surface has an attractive portion that does intersect the ground state potential surface. In C_s symmetry, the crossing is avoided and thus the system exhibits a conical intersection. A very nice *ab initio* analysis of wavefunctions in the vicinity of the conical intersection in the simple case of $Na^* + N_2$ quenching shows significant charge transfer from the metal atom to the nitrogen molecule, in geometries in which the N–N bond is stretched from its equilibrium distance [123]. The transfer of electronic energy proceeds via internal conversion to highly vibrationally-excited levels of the ground electronic state of the system.

This mechanism readily generalizes to alkaline earth monocation–solvent interactions. To our knowledge, *ab initio* calculations to probe important regions of the potential surfaces for the Sr^+-based reactions have not been carried out. However, Kleiber and co-workers have performed experimental and theoretical studies on related Mg^+ systems that probe the nature of the key interactions

[124–127]. Their work shows clearly that conical intersections between excited states and the ground state facilitate dissociation and resultant internal excitation of the fragments. Those studies lend strong support to the applicability of the bond-stretching attraction model to alkaline earth–solvent clusters.

The bond-stretching attraction model provides insight into the physics of electronic quenching, and focuses attention on the coupled issues of electron transfer and vibrational excitation. *Ab initio* quantum mechanical calculations on model systems are essential in understanding the nature of the valence electron distributions in systems isoelectronic with alkali metal–solvent systems. These calculations will be discussed below. The nature of the internal energy distributions of the products of cluster ion photodissociation is more directly amenable to experimental tests. We are unaware of direct pump–probe or state-to-state measurements of product fragment internal state distributions in metal ion–polar solvent systems. Nevertheless, some recent data from our group [27] provide significant insight into the dissociation mechanism and confirmation of the notion that products of photodissociation processes are vibrationally excited.

A careful analysis of the fluence dependences of parent ion depletion and formation of successive generations of product ions is essential in interpreting the branching ratios for daughter ion and higher generation fragment production. The $Sr^+(CH_3OD)_n$ system provides an excellent case study. Fluence dependence studies [27] in this system illustrate that the primary reaction channels given in equations (2)–(4) and shown in the reaction coordinate diagram of figure 5 are single-photon processes. The fluence dependences for the 'combination channels', in which a primary product is accompanied by loss of one or more solvent molecules are consistent with higher order absorption processes. For example, in figure 4, the mass spectrum of products for the $n=2$ cluster shows that the combination channels –2L, –(L + Me), and –(L + D) have a quadratic dependence on fluence. As required by energy conservation, we treat the combination channels in figure 4 as the one-photon products of a cluster $Sr^+(CH_3OD)$ that itself arises from single photon absorption by $Sr^+(CH_3OD)_2$. We therefore interpret the first-generation cluster denoted by –L as the residual parent of the combination channels. The signals from the individual second-generation fragment channels are normalized to the total charge of the residual parent. Thus, the ligand loss peak is treated as the residual parent ion for the subsequent photon absorption event.

Fluence dependences for formation of higher generations of fragments are also consistent with a sequential photon absorption mechanism and lead to the global scheme shown in figure 15. The scheme shows that the single-photon products in which the metal ion has been oxidized, i.e. the –D and –Me channels, do not absorb a second photon of the same frequency that produced them. Consequently, the only pathway by which combination channels can be formed is through intermediates that have lost a solvent by single photon absorption. Combination channels in which a primary product is accompanied by m solvent molecules must arise from $(m+1)$-photon absorption by a parent incorporating the original m solvents. The fluence dependence studies are consistent with this picture.

By applying charge conservation as required by the sequential one-photon absorption scheme to experimental data like those shown in figure 6, we can extract photodissociation spectra and branching ratios for the intermediate clusters $Sr^+(CH_3OD)_{n-1}$, $Sr^+(CH_3OD)_{n-2}$, etc. As an example, figure 16 shows the intensity distribution of the second generation fragments from $Sr^+(CH_3OD)_2$ normalized by

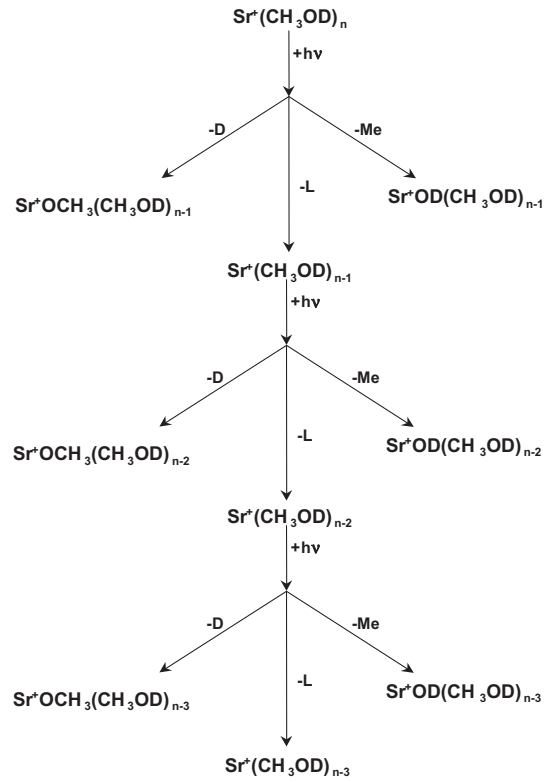

Figure 15. Schematic depiction of the proposed sequential absorption mechanism, illustrating that higher-order generations are accessed only through Sr^+–(methanol) species. Figure reprinted from reference [27] with permission.

treating the –L daughter ion, i.e. $Sr^+(CH_3OD)^*$, as the residual parent. The notation $Sr^+(CH_3OD)^*$ indicates that the parent ion yielding the spectrum is itself produced by photolysis. In essence, figure 16 plots the one-photon photofragment signal for monomer ions produced by single photon dissociation of cold dimer ions. The bond-stretching attraction model [121] predicts that the nascent monomers created by photodissociation are internally excited, and consequently the spectrum in figure 16 reflects the action spectrum for 'hot' monomers.

Comparison of the 'hot' monomer spectrum in figure 16 with its 'cold' counterpart in figure 6 shows that internal excitation in the parent cluster results in a significantly broadened and red-shifted spectrum. Qualitatively, this is precisely what one would expect as 'hot bands' dominate the absorption process. The partially resolved feature at 18000 cm^{-1} appears to originate from the much sharper band assigned to 4dπ excitations. One can still see vestiges of the 5pπ excitations near 20000 and 22000 cm^{-1}. Figure 17 shows the results of this analysis applied to dissociation of the trimer ion, in which sequential absorption of two photons prepares a very highly vibrationally excited monomer ion, denoted $Sr^+(CH_3OD)^{**}$, that absorbs an additional photon. In the spectrum of this highly-excited species, we see that the intensity maximum occurs near 14000 cm^{-1}, significantly red-shifted from the absorptions of the cold clusters or those prepared by only a single sequential absorption step. In fact, the colder clusters have very little absorption

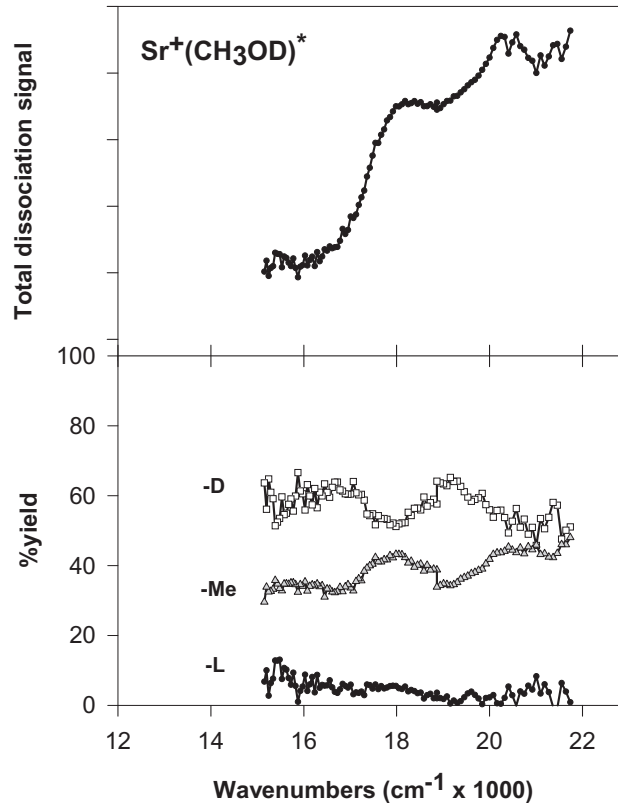

Figure 16. Upper panel: $Sr^{+}(CH_3OD)^*$ total photodissociation signal for formation of all product channels. The signal at each photolysis wavelength arises from the first-generation fragments coming from $Sr^{+}(CH_3OD)^*$ produced by single-photon dissociation of $Sr^{+}(CH_3OD)_2$. Lower panel: branching fractions for the –D, –Me, and –L channels relative to the residual parent $Sr^{+}(CH_3OD)$ arising from single photon absorption in the dimer. Figure reprinted from reference [27] with permission.

at all in this spectral region. We note that the two absorptions attributed to excitation of 5pπ states are still clearly in evidence in this spectrum.

The red shifts that the spectra of $Sr^{+}(CH_3OD)^*$ and $Sr^{+}(CH_3OD)^{**}$ exhibit relative to the 'cold' cluster are qualitatively what one expects for photoexcitation from 'hot bands'. However, even stronger support for the interpretation of these spectra as coming from species with increasing levels of vibrational excitation comes from considering the product branching ratios. In general, increasing levels of parent ion vibrational excitation enhance the formation of the –D and –Me products, both of which occur over exit channel barriers in excess of the reaction endothermicity, as shown in figure 5. Reactant vibrational excitation is often effective in surmounting potential energy barriers to reaction [128–131], principally under conditions where the excitation induces molecular motion along critical reaction coordinates. In the bottom panel of figure 16, we see that an increase in cluster internal excitation preferentially enhances the cross-sections for the –D and –Me reactions relative to simple solvent evaporation. In particular, the –D channel, which dominates in the 4d-based electronic states of the 'cold' cluster, owing to favourable orbital size considerations that allow O–D bond activation, now gains

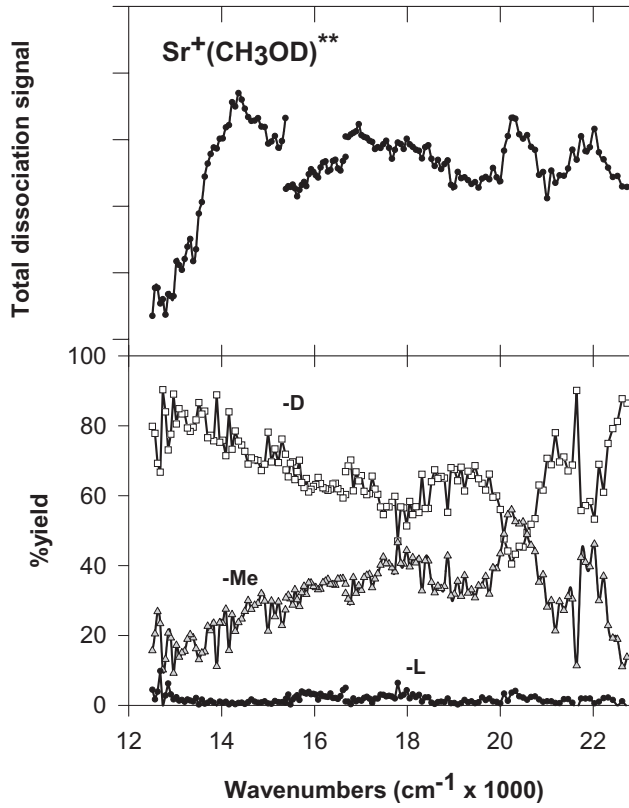

Figure 17. Upper panel: $Sr^{+}(CH_3OD)^{**}$ monomer total photodissociation signal for formation of all product channels. The signal at each photolysis wavelength arises from the first-generation fragments coming from $Sr^{+}(CH_3OD)^{**}$ produced by sequential two-photon dissociation of $Sr^{+}(CH_3OD)_3$. Lower panel: branching fractions for the –D, –Me, and –L channels relative to the residual parent $Sr^{+}(CH_3OD)$ arising from two-photon absorption in the trimer. Figure reprinted from reference [27] with permission.

cross-section in the higher energy 5pπ-based states. The most impressive effect of vibrational excitation is seen in the branching ratios shown in the lower panel of figure 17: the data show that solvent evaporation is suppressed even further. The –D and –Me channels continue to compete favourably in the 5pπ region of the spectrum, but now, in the very low energy region of the spectrum where the parents have the highest level of internal excitation, the –D product is by far the favoured product. The difference in enhancement of –D and –Me is consistent with the difference in barrier height between the channels. While both channels are enhanced relative to the branching ratios observed in the cold monomer, the –D channel is much more strongly affected. Although the dynamical origins of this enhancement are not understood at present and will require theoretical explication, it is sensible to attribute the enhancement of O–D bond cleavage with enhanced D-atom migration associated with O–D vibrational excitation.

Both the spectroscopic data and the product branching ratios for $Sr^{+}(CH_3OD)$ clusters prepared by ligand loss via sequential photon absorption are consistent with the picture that the dissociation process converts electronic energy into

vibrational excitation. Theoretical work to help interpret the evolution of absorption spectra with increasing levels of internal excitation, as well as dynamical studies that probe the effects of specific molecular motions on product branching ratios, will help provide a firmer understanding of the electronic to vibrational energy transfer process.

7. Evolution of electronic states in clusters

Size-dependent photodissociation studies of ionic clusters comprised of polar solvent molecules surrounding a singly-charged alkaline earth core raise a number of structural and dynamical issues. In addition to the question of the role of the bond-stretching attraction model in mediating electronic to vibrational energy transfer, general issues concerning chemical reactivity and specific questions of metal atom oxidation and electron transfer become important. The evolution of the electronic states of these species as a function of cluster size is the critical physical parameter that provides a unifying interpretation of the data. The same issue arises in a number of other physically related systems that have been the subject of spectroscopic probes and *ab initio* theoretical treatments. For example, measurements of the ionization potentials as a function of cluster size have provided important probes of the isoelectronic clusters based on alkali metals [132–135] and the Rydberg radical NH_4 [108]; depletion spectroscopy has also yielded the absorption spectra of some of these same species. Photoelectron spectroscopy of alkali anions solvated by variable numbers of NH_3 or H_2O molecules has also revealed important structural details of the electronic states of the solvated alkali metals thereby produced [134]. All of these studies reveal a cluster size-dependent compression of the energy level structure based on the one-electron 'core'. It is helpful to summarize the results of these related experiments and theoretical methods in order to understand the underlying principles operative in these systems.

The size dependence of the ionization potentials in clusters formed by solvating the neutral alkali atoms Li, Na, and Cs by NH_3 and H_2O provides a case study. Classical electrostatic models [136–140] predict that electron binding energies in such clusters approach the bulk value as a function of R^{-1}, where R is the cluster radius. For a cluster comprised of n monomers, each of radius r_s, the cluster radius can be defined as $R = n^{1/3} r_s$. Thus a classical model predicts that electron binding energies should scale with $n^{-1/3}$, approaching the bulk work function as $n \to \infty$. As reported by the groups of Fuke and co-workers [132–134], and Hertel *et al.* [135], a plot of the ionization potentials of clusters $M(NH_3)_n$ vs. $n^{-1/3}$ approaches linearity for $n \geq 6$–8 and extrapolates at large n to a metal-independent value of 1.47 eV. This value is remarkably close to the bulk photoemission threshold for liquid ammonia and metal–ammonia solutions [141]. Similar studies of these same metals solvated by H_2O reveal that for even smaller cluster sizes, $n \geq 4$, the ionization potential reaches a constant value of 3.1 eV, which represents the bulk photoelectric threshold for ice [142]. The experiments indicate that electron emission in the large cluster limit is independent of metal, but dependent on solvent. The fact that recent results of Bowen and co-workers on the size-dependence of the vertical detachment energies for $(NH_3)_n^-$ [143] and $(H_2O)_n^-$ clusters [144] produce values similar to those observed in the solvated metal atom systems suggests that electron detachment occurs from a negatively-charged solvent cluster unit in the latter systems. Such an observation provides direct evidence that spontaneous ionization, in which the metal valence

electron is removed from its atomic ion core and bound by a collection of solvent molecules in the cluster, occurs in the metal atom–solvent systems. The view that anionic solvent clusters are embryonic forms of solvated electrons that mature to the bulk condensed phase species suggests that the nature of the spontaneous ionization process in solvated metal atom clusters illuminates the nature of the bulk state.

An important distinction between metals solvated by NH_3 or H_2O originates in the relative magnitudes of the solvent–solvent interactions. Intermolecular interaction in ammonia are observed to be approximately tenfold weaker than in water [145], a phenomenon reflected in the propensity of the latter solvent to engage in highly networked hydrogen bonding interactions. This fact is responsible for significant differences in the spectral and structural features observed in clusters based on the two solvents. *Ab initio* calculations [99, 146–150] have shown, for example, that alkali metal–water clusters exhibit a saturation of the IP for $n > 4$, arising from a highly-structured molecular shell comprised of four solvent molecules, which excludes the valence electron from this inner 'hydration cavity'. The valence electron is effectively delocalized in a surface state. In metal–ammonia clusters, the less structured solvent dipole network allows the valence electron to interact with solvent molecules in the inner solvation shell and on the cluster surface [100]. In both cases, the metal-solvent systems exhibit so-called Rydberg-like ion-pair states, but the $n^{-1/3}$ extrapolation of the IP toward the bulk value is more gradual in the ammonia case.

Theoretical calculations provide insight into the changes in electronic structure around the alkali atom as a function of the number and identity of solvent molecules. The earliest *ab initio* calculations by Hashimoto and Morokuma [100] on metal–solvent systems, performed on $Na(NH_3)_n$ clusters, show that the singly-occupied molecular orbital (SOMO) in which the metal valence electron resides undergoes characteristic changes in size and shape with increasing number of solvent molecules. The calculations show that the most stable configurations for $n \geq 4$ are interior structures with the metal atom surrounded by four or five ammonia molecules in the first solvation shell. The SOMO increases in size and diffusive character with increasing number of solvents, and has a clear bonding character in the $n = 4$ cluster. That bonding character results in a slight shortening of the Na–N bond length in the neutral cluster (2.454 Å) relative to the ionic species (2.476 Å). More detailed calculations on small clusters based on Li and Na solvated by H_2O show that the SOMO looks like an sp-hybrid orbital directed away from the solvent molecules [132, 134]. In the range from 6 to 8 solvent molecules, the SOMO breaks up into a surface state with amplitude on each of the solvent molecules, while around 9 solvents, the SOMO is localized in the volume defined by adjacent O–H dipoles, a so-called molecular 'tweezers' state formed by two or three dangling O–H bonds not involved in hydrogen bonding. *Ab initio* calculations by Iwata and co-workers [151] suggest that these three regimes correspond to 'quasi-valence', 'surface', and 'semi-internal', and it is this last state, similar to the 'tweezers' state described by Reinhard and Niedner-Schatteburg [92–94] in the context of ion-pair formation in $Mg^+(H_2O)_n$ clusters, that localizes the electron within the solvent, independent of metal. The calculations draw attention to the nature of the cage-like structure that constrains the electron. Such states have been identified in early *ab initio* work on the water hexamer anion [152, 153], and in experimental studies of the infrared spectra of $(H_2O)_n^-$ clusters [154]. The semi-internal 'tweezers' states have not

been observed in analogous ammonia-based clusters; perhaps the significantly weaker solvent–solvent interactions in ammonia preclude the formation of a structured matrix of dipoles to trap the excess electron.

The *ab initio* calculations in conjunction with size-dependent ionization potential measurements all support the idea that the ground states of these metal–solvent clusters with single valence electron metal cores achieve ion-pair character in a particular size regime. Specific details of the solvent–solvent interactions give different character to clusters based on water as compared with ammonia. Although many of the calculations avoid the use of the term 'Rydberg state' to describe such states, inasmuch as detailed analysis of the SOMO indicates a shape much more complex than that of spherical symmetry, the states are termed 'one-centre ion-pair' states in some of the calculations, and their primary manifestation is in the size-dependent reduction of ionization potential. Interestingly, Fuke and co-workers [89] point out that the SOMO in Ca^+ is spherically symmetric, likely resulting from sd hybridization; a similar situation should hold for Sr^+. This situation contrasts with the directed SOMO lobes with sp character in the better-studied Mg^+ systems.

Ionization potential measurements probe the gap between the cluster ground state and the ionization continuum. Complementary probes of the bound state level structure of the metal in the presence of variable numbers of solvent molecules provide additional insight into the nature of spontaneous ionization, and can be achieved with photoelectron spectroscopy of anions detaching to the neutral species of interest. Photoelectron spectroscopic studies of the cluster anions $M^-(H_2O)_n$ and $M^-(NH_3)_n$ provide information about the energies of the ground and bound excited states of the clusters as a function of cluster size. In the $Li^-(NH_3)_n$ and $Na^-(NH_3)_n$ systems, the vertical detachment (VDE) energies to the 3 ^{2}S and 2 ^{2}P states in the former, and the 3 ^{2}P and 3 ^{2}S states in the latter, decrease with cluster size [134]. This behaviour occurs in concert with the decrease in ionization potential and provides a consistent picture of spontaneous ionization induced by the solvent environment. The $Na^-(H_2O)_n$ systems also exhibit behaviour consistent with the IP measurements in the neutral systems, showing that the VDE's track the IP's, reaching constant values for $n \geq 5$. The combination of spectroscopic probes and *ab initio* calculations shows that expansion of the SOMO occurs with increasing solvation. The details of the shape of the SOMO depend sensitively on the solvent identity, with clusters based on water showing a more highly constrained valence electron distribution in which electron density is excluded from the volume occupied by the four solvent molecules in the first solvation shell.

A global consideration of all the experimental data discussed here suggests a clear pattern: the electronic states that are involved in the initial absorption of alkaline earth metal ion–polar solvent clusters are based on the atomic states of the core metal. For some electronic states in singly-solvated Mg^+ cluster ions, particularly strong metal–ligand repulsions blue-shift the electronic states of the cluster relative to the atomic ion transitions. However, the energy gaps decrease relative to the atomic ion in doubly-solvated and larger clusters. In Ca^+- and Sr^+-based clusters, the electronic absorptions are always red-shifted relative to their atomic ion counterparts. These red shifts appear to reach maximum values at solvent numbers near four solvent molecules for Mg^+, and six to eight molecules for Ca^+ and Sr^+. Additional solvents appear to make very small contributions to spectral red shifts; the much smaller metal–solvent interactions implied by these red shifts suggest that these molecules are bound in a second solvent shell.

This general size-dependent motif for the electronic absorptions in solvated alkaline earth ion clusters carries over to the behaviour of the absorption spectra of solvated alkali systems, a point that is made quite strikingly in the comparison among the absorption spectra of the isoelectronic species $Mg^+(NH_3)_n$, $Na(NH_3)_n$, and $NH_4(NH_3)_n$. Such absorption spectra coupled with complementary vertical detachment energy measurement in solvated alkali anion clusters demonstrate clearly that the energy gaps of the atomic state-based ground and electronically excited levels of the clusters decrease with cluster size. That picture is augmented by ionization potential measurements of size-selected alkali atom clusters that show a decrease in IP with increasing cluster size.

The electronic states of these clusters have been the subject of a number of theoretical calculations carried out to understand how cluster properties ultimately relate to properties of the bulk. Much of that discussion has considered the metal-solvent electron transfer processes accompanying the formation of bulk solvated electrons, and a number of simple models developed for condensed phase processes may be applied profitably to the cluster case. The polar solvent interactions that appear to induce electron transfer processes that drive the valence electron away from its core nucleus raise the general issue of spontaneous ionization and the interaction of valence electronic states with charge transfer or ion-pair states, especially the effect of variations in the solvent environment. We therefore ask about the nature of physics common to all of these systems.

The principal issue that must be addressed first is the question of how the energy cost of spontaneous ionization is compensated for by solvation. As an initial approach to this problem, we consider a Born thermodynamic cycle for estimating the energies of charge transfer, i.e. ion-pair, states as a function of cluster size. This discussion is based on the venerable Franck–Platzman model [155] for calculating charge transfer to solvent (ctts) spectra in condensed phase systems [156]. This model employs a thermodynamic cycle to account for the manner in which the energy expended to transfer charge in a donor acceptor complex, i.e. $(D \cdot A) \rightarrow (D^+ \cdot A^-)$, is compensated for by solvation of the cationic and anionic entities in the products. The cycle evaluates the separation ΔE_{CT} between the ground state and a charge transfer excited state in which the solvent have reorganized about the two-centre (dipolar) charge distribution of the excited state.

$$\begin{array}{ccc} M^+(L)_n & \xrightarrow{\Delta E_{CT}} & M^{2+}(L)_{n-m}(L)_m^- \\ \Big\downarrow -\Delta H_{solv}^{(+)} & & \Big\uparrow \Delta H_{solv}^{(+2)} + \Delta H_{solv}^{(-)} + E_{pol} \\ M^+ + n\,L & \xrightarrow{IP - E_{Coulomb}} & (M^{2+} \cdots e^-) + nL \end{array}$$

The cycle is written for second ionization potential processes applicable to alkaline earth species, but may be generalized to first ionization potential processes in alkali atoms. The first term in the cycle, $-\Delta H_{solv}^{(+)}$, accounts for the energy of solvation of the singly-charged ion by n ligands. The second term accounts for the energy required to move a valence electron to a specified distance in the coulomb field of the M^{2+} core, creating a two-centre charge distribution. The third term evaluates the separate solvation energies of the cation and the electron, and the polarization interaction between the oppositely-charged sub-cluster moieties in the full cluster. Although many approximations go into this calculation, the energetics are driven by

the fact that each successive solvent molecule stabilizes clusters based on the singly-charged atomic ion core by 15–25 kcal mol^{-1}, but the energy gained from solvating the doubly-charged ion lowers the charge transfer state energy by 25–35 kcal mol^{-1} per solvent molecule. Thus, ΔE_{CT} appears to decrease monotonically from ~60 kcal mol^{-1} for the triply-solvated Sr^+ to 30 kcal mol^{-1} for the hexamer. The absolute magnitudes of the energy gaps depend on the appropriate ionization potentials of the metal. For the singly-charged alkaline earth species Mg^+, Ca^+ and Sr^+, the second ionization potentials are 15.0, 11.87 and 11.0 eV respectively. Consequently, the relative magnitudes of the charge transfer energy gaps for a given cluster size should be ordered as $Mg^+ > Ca^+ > Sr^+$, although the larger solvation energies of the clusters of the lighter metals will partially compensate the effects of IP.

The Born cycle picture demonstrates that the ion-pair states lie above the ground state configuration based on the ^2S atomic ion core, but are comparable in energy to the excited states based on $^2P \leftarrow {}^2S$ transitions. Rather than being accessed directly by spectroscopy, these ion-pair states may be mixed into valence state wavefunctions by electron–electron repulsion or vibrational interactions. The mixing coefficients depend inversely on the energy separation of the relevant states, and we expect charge transfer character to manifest itself first in the more highly excited states of small clusters. As the ion-pair states drop in energy, the lower-lying excited states and the ground state acquire more charge transfer character.

The Born cycle picture suggests that the charge transfer nature of both the ground and excited state wavefunctions should evolve with increasing cluster size. Electronic structure calculations that probe the radial distribution function of the valence electron, i.e. the SOMO, can assess this mixing. An early path integral Monte Carlo (PIMC) calculation by Martyna and Klein [157] on $Sr^+(NH_3)_n$ showed that the radial distribution function for the valence electron in such clusters expanded monotonically with size. In the range near $n = 6$, the expansion of the ground state electron density was attributed to Rydberg character induced by solvent lone pair interactions with the metal valence electron. Similar behaviour was also predicted in *ab initio* calculations by Harrison and co-workers on the Li(9-crown-3)$_2$ system [158], in which the lone-pair interactions of the crown ether oxygen atoms with the lithium atom valence electron 'squeezed' it into a Rydberg state.

The calculations described earlier on the related $Mg^+(H_2O)_n$ system, which showed clear evidence for the formation of a solvent-separated ion-pair state for $n \geq 10$, provide a more complete picture of the size-dependence of the SOMO in this system. Figure 18 shows the results of this analysis as applied to the ground state SOMO [92]. The SOMO clearly expands with increasing cluster size, even for the addition of the first solvent molecule. This result is distinguished from the behaviour exhibited by the PIMC calculations on $Sr^+(NH_3)_n$, in which no significant difference between the SOMO's of the atomic ion and the singly-solvated cluster ions is observed.

The spectroscopic motif exhibited by polar solvent one-electron atomic core clusters contains direct experimental insight into the nature of the ground state SOMO in such species. We can make this connection between cross-section and ground state electronic properties by considering frequency moments of the absorption cross-section. In the case where an atomic or molecular system is reasonably well-described as a one-electron system, i.e. the single valence electron is in an orbital that has minimal interaction with the core, measuring the complete

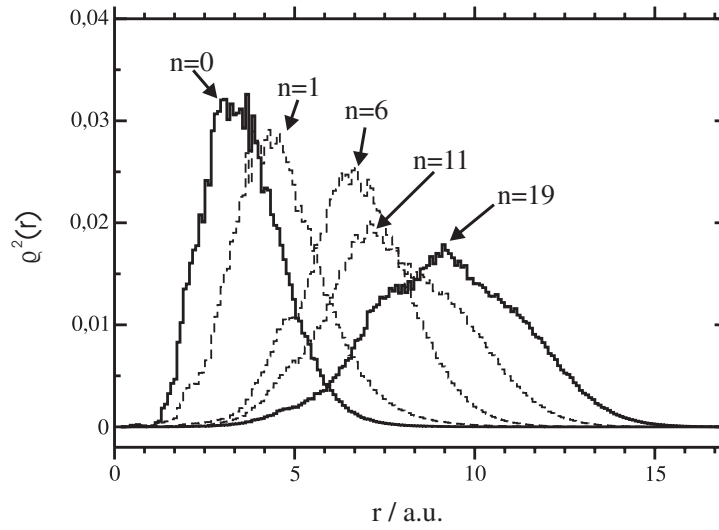

Figure 18. Radial distribution functions for the SOMO in $Mg^+(H_2O)_n$. Figure reprinted from reference [92] with permission.

absorption spectrum allows us to apply a class of useful sum rules [159] on intensities or oscillator strengths f_{0n}. These sum rules have played a useful role in bounding the moments of cross-sections for many physical processes [160]. The relationships have also been applied profitably to the bulk absorption spectra of solvated electrons, with the objective of probing the length scale over which the electron is localized in condensed matter [35].

In the alkaline earth cation systems in particular, where the atomic ion is isoelectronic with alkali atoms and the cluster ground electronic states have significant atomic ion parentage, these sum rules have a particularly pleasing interpretation. The sum rules can be written in the following form:

$$S(k) = \sum\nolimits_n f_{0n} E_n^k \tag{5}$$

In the discrete case, the summation extends over all excited n states of energy E_n carrying oscillator strength f_{0n} from the ground state. Equation (5) can be generalized to systems with continuous spectra, and since the absorption cross-section $I(\omega)$ is proportional to the oscillator strength per unit energy, these sum rules correspond to frequency moments of the complete absorption spectrum. In the case of $k = 0$, the sum is the familiar Thomas–Reiche–Kuhn sum rule, with $S(0) = N$, the number of valence electrons in the system. For our purposes, the critical sum rule is the one for which $k = -1$. A very simple manipulation of the absorption cross-section in the one-electron approximation, exploiting the completeness of the basis functions, demonstrates that $S(-1)$ is directly proportional to $\langle 0|r^2|0\rangle$ or $\langle r^2\rangle$, the mean square radius of the electron probability distribution in the ground electronic state. We expect the one-electron approximation to be reasonably good for species with alkali metal electronic configurations and for their clusters with closed shell, negative electron affinity solvents such as H_2O and NH_3.

The application of spectral moments to solvated electron systems has been extended to cluster anions; in these systems, the objective is to determine whether

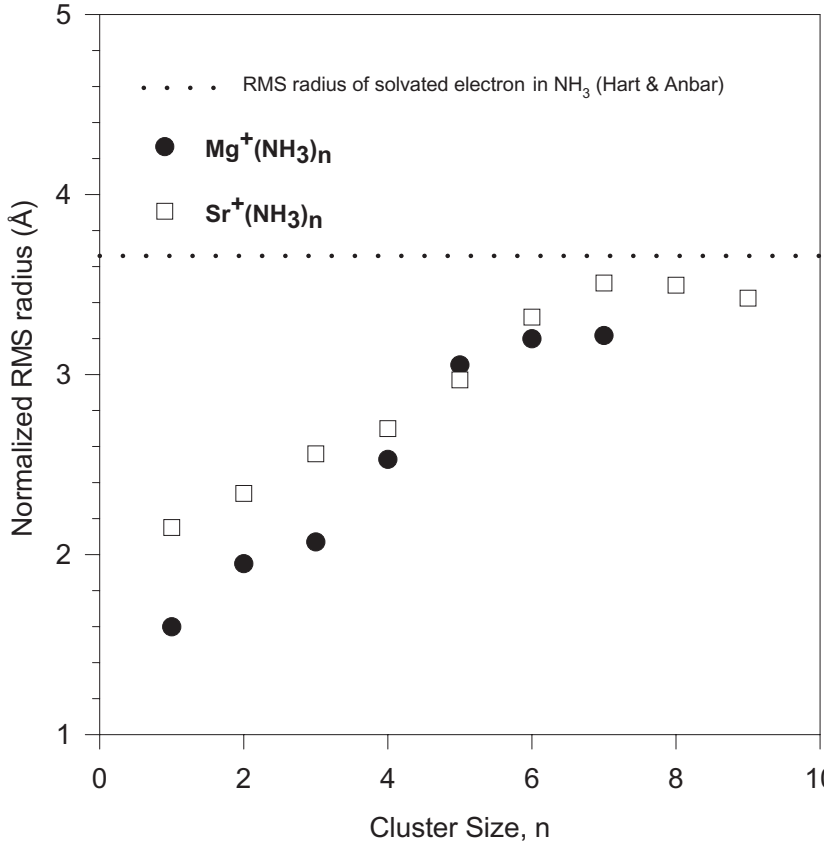

Figure 19. Results of spectral moment analysis of $\langle r^2 \rangle^{1/2}$ from the dissociation spectra of $Mg^+(NH_3)_n$, $Sr^+(NH_3)_n$. The horizontal line indicating the bulk limit for the solvated electron in ammonia is from HART, E. J., and ANBAR, M., 1970, *The Hydrated Electron* (New York: Wiley-Interscience).

the excess electron is bound on the surface or is confined to an interior state of the cluster, and what the physical dimensions of such a state are [161–163]. In the case of one-electron atomic or molecular 'cores' surrounded by polar solvent molecules, calculation of $S(-1)$ allows $\langle r^2 \rangle^{1/2}$ for the SOMO to be extracted from size-dependent absorption spectra. Qualitatively, one expects the mean square radius of the ground state SOMO to evolve toward a limit consistent with bulk values.

Figure 19 shows the results of this analysis applied to the dissociation spectra of $Sr^+(NH_3)_n$, for $n = 1$–9, from figure 8, and $Mg^+(NH_3)_n$, for $n = 1$–7, from figure 7. The experimentally-derived values of $\langle r^2 \rangle^{1/2}$ increase monotonically with increasing cluster size, and approach a limiting value consistent with the bulk limit. Although one might have argued that this result reflects d–p mixing in the Sr case, the identical behaviour of the Mg system, in which such mixing is absent, suggests a deeper physical interpretation.

This simple, but physically appealing result can be discussed in the context of *ab initio* calculations on related systems. The recent calculations on the nature of the SOMO in $Mg^+(H_2O)_n$ show that the cluster size-dependence of the ground state electron density is qualitatively consistent with results like those of figure 19 [92–94].

The SOMO radius plot exhibits some structure more complex than simple monotonicity, correlating with different size regimes in which both contact and solvent-separated ion pairs, i.e. states exhibiting spontaneous ionization, appear to be formed, but the basic increase with cluster size holds.

The mechanism for spontaneous ionization appears to involve the mixing of ion-pair states into valence state wavefunctions. That mixing should manifest itself as a spatial expansion of the probability density of the electron [157]. The Born cycle analysis of clusters shows that the requisite ion-pair or charge transfer states fall in energy with increasing cluster size. According to this picture, the mixing should first exhibit itself in excited electronic states of smaller clusters before it reveals itself in the ground states of larger clusters. The spectral moment analysis integrates the observed spectrum of a given species over all excited electronic states, therefore revealing only ground state information. However, the results of *ab initio* calculations may be employed to estimate the radial electron density distributions and their moments both in ground and excited states. The recent calculations of Yoshida [65] on the $Mg^+(NH_3)_n$ system show that the calculated ground state values of $\langle r^2\rangle^{1/2}$ agree with the experimentally-derived values plotted in figure 19 within about 10%. The size-dependent growth in $\langle r^2\rangle^{1/2}$ has contributions from metal–ligand repulsions that 'squeeze' the electron out of the volume occupied by the solvent molecules, as well as from interactions that drive the electron into a spherically symmetric one-centre ion-pair Rydberg state. Yoshida *et al.* [65] show that the former contributions can be assessed by evaluating $\langle z\rangle$ for the SOMO. The result of this analysis shows that in tetrahedral $Mg^+(NH_3)_4$, $\langle z\rangle = 0$, demonstrating that expansion of the electron density arises from the growth of one-centre ion-pair character of the cluster. The analysis also shows that values of $\langle r^2\rangle^{1/2}$ for excited states of the $n=3$ and 4 clusters based on the 3p orbitals of Mg^+ are almost twice the size of the ^2P state of the bare ion. The authors attribute this behaviour to increased charge transfer character in the excited states, as observed in the solvation of alkali atoms [89, 164, 165]. This increased charge transfer character in the excited states of $Mg^+(NH_3)_n$ for $n > 2$ leads to stronger binding in the excited states of the larger clusters, thus increasing absorption red shifts. By removing the effects of d–p mixing, the $Mg^+(NH_3)_n$ systems confirm that the red shifts seen in the dissociation spectra of the larger clusters arise from increasing ion-pair character of ground and excited state wavefunctions. The authors conclude by stating that despite the significant differences in the electronic structure of Mg^+ and Sr^+, the behaviour of the spectra is independent of metal, and therefore provides information on incipient solvated electron systems.

The evolution of the electronic states of effective one-electron species in the field of a small number of polar solvent molecules provides a unifying picture for a wide array of chemically similar species. However, clusters that contain more than one such effective one-electron species also provide interesting challenges for experiment and theory. The final section discusses one such example.

8. Exotic systems: $Sr^+(ND_3)_nD_x$

The cluster systems discussed to this point can be characterized as having a single one-electron core chromophore whose behaviour is influenced by the local solvation environment. The photochemistry of these clusters reveals the modifications of the electronic distribution as solvent molecules are added stepwise to the

cluster. The strontium–ammonia system provides a glimpse of clusters that have more than one chromophore. The initial realization that such systems might be probed with mass spectrometry and laser photoabsorption spectroscopy came from the mass spectral data of figure 3, indicating that strontium–ammonia clusters with 12 or more solvent molecules also bind from one to four excess deuterium atoms. Studies in which the clusters were reacted with an external source of NO, a hydrogen/deuterium atom scavenger, suggested that D atoms were 'etched' from the surface of the clusters with $x = 2$, 3, and 4, but not $x = 1$. Clusters with only a single excess D atom were not affected by the added NO, suggesting that the first D atom in the cluster is bound in the interior of the cluster. Control experiments with He showed no reactivity with excess D-atom containing species [63].

The scavenging experiment with NO suggests that the $Sr^+(ND_3)_nD_x$ species with two or more excess deuterium atoms ($x \geq 2$) are chemically distinct from species with only a single excess deuterium atom. This apparent difference in reactivity can be probed spectroscopically. Photodissociation spectra for $Sr^+(ND_3)_{12}D_{1,2,3}$ and $Sr^+(ND_3)_{13}D_{1,2,3}$ clusters are shown in figure 20. The spectra have several interesting features. Each of these clusters has a strong, broad absorption band around 11000 cm^{-1}, and a much weaker absorption band at 18000 cm^{-1}. Both bands shift 3000 cm^{-1} higher in energy as x varies from 1 to 3, i.e. as the number of excess deuterium atoms increases. Clusters containing at least two excess deuterium atoms (i.e. $x \geq 2$) have an additional absorption band peaking at 6200 cm^{-1}, a feature absent in clusters containing only one extra deuterium. It appears that the

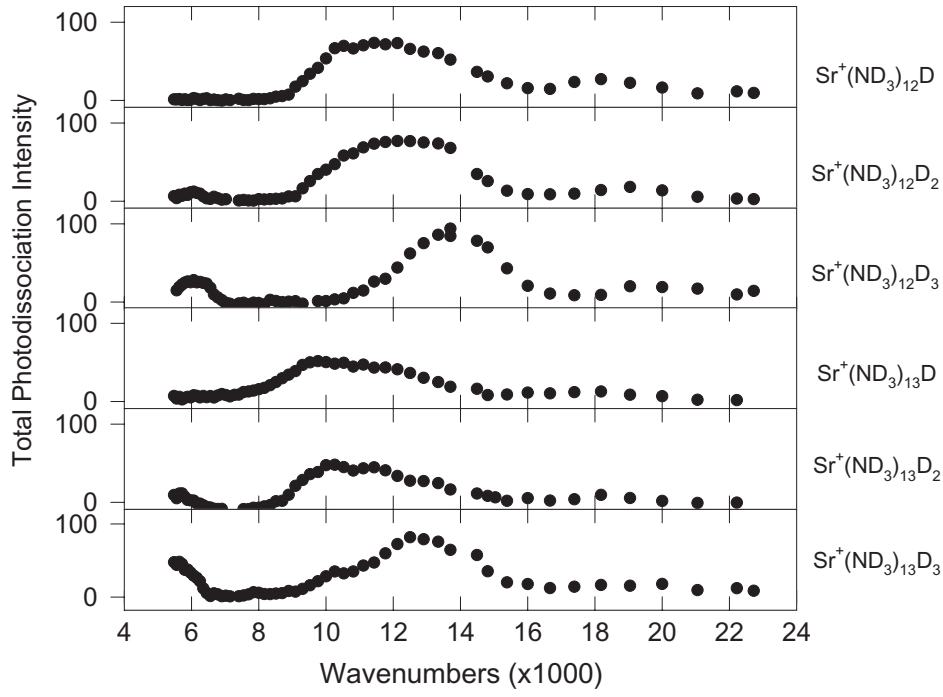

Figure 20. Upper three panels: photodissociation spectra for $Sr^+(NH_3)_{12}D_x$, for $x = 1$, 2, and 3. Lower three panels: photodissociation spectra for $Sr^+(NH_3)_{13}D_x$, for $x = 1$, 2, and 3.

$x = 2$ and 3 species have a chromophore that is absent in the $x = 1$ species. Thus, the first excess deuterium atom appears to add to the cluster in a location structurally and chemically distinct from the second and third. The lack of reactivity with NO suggests that the first excess deuterium atom is located in the cluster's interior, where it is inaccessible to NO.

The previous observations make it tempting to attribute the absorption band peaking at 6200 cm^{-1} to clusters that have two or more excess deuterium atoms. The broad features that are present for all clusters are likely attributable to a chromophore in the interior of the cluster that incorporates the first excess deuterium atom. One possibility for satisfying the second of these conditions is to consider an alkaline earth hydride cation chromophore. Alkaline earth metal hydride cations, despite being stable species, have received relatively little attention. Only a few reports of the ground state properties of SrH^+ exist [166–170]. The hydrogen is bound by ~2 eV [167, 169], while the electron affinity (5.58 eV) [166] is very close to that of the metal ion, Sr^+. Experimental determinations of the electronic properties exist only for MgH^+ [171], while some theoretical predictions on the general electronic structure were made by Schilling *et al.* [167]. The only known study that addresses the issue of the electronic spectra of such species is an *ab initio* calculation on CaH^+ by Boutalib *et al.* [172]. That study suggests by analogy that it is plausible to attribute the two broad features in the visible region of the spectrum in figure 20 to two allowed transitions of a metal hydride species, i.e. SrD^+.

Assigning the low energy feature of the spectra for clusters with at least two excess deuterium atoms was aided by considerations of the photochemistry of ammonia clusters. Recent work to elucidate the dynamics of formation of protonated ammonia cluster ions in the multiphoton ionization of ammonia clusters [173–175] has shown that predissociation of NH_3 in the $\tilde{A}$ electronic state produces hydrogen atoms that form a transient ammonium radical that undergoes subsequent ionization. Recent calculations by Boldyrev and Simons [176] suggest that mixed valence-Rydberg bonds can be formed between alkali metals and the NH_4 radical, and that the transient species formed by this electron pair bond may decay to yield a metal hydride and ammonia. One would expect even stronger bonds to be formed between an alkaline earth ion and the Rydberg molecule, and in the case of laser vaporization of Sr in the presence of ammonia clusters, its is reasonable to expect the following reaction to occur:

$$Sr^+ + ND_4 \rightarrow SrD^+ + ND_3 \tag{6}$$

Reaction (6) provides a mechanism for the formation of the SrD^+ cluster core that we have speculated on as the carrier of the broad bands near 11000 and 18000 cm^{-1}. In addition, one might expect the well-known solvated ammonium radicals $NH_4(NH_3)_n$, or their isotopically labelled analogues, $ND_4(ND_3)_n$, to be formed as well. By accretion of such species on the surface of a growing cluster produced by laser vaporization, clusters of the form $Sr^+(ND_3)_nD_{1,2,3}$ might be formed.

This speculative proposal receives strong confirmation in the comparison of the weak spectral feature observed in $Sr^+(ND_3)_{12}D_x$ clusters with at least two excess deuterium atoms and the absorption spectra of $NH_4(NH_3)_n$ clusters. In fact, the spectral feature shown for the $x = 2$ species in figure 9 is perfectly congruent with the electronic absorption spectrum of $NH_4(NH_3)_4$ shown in figure 14.

Despite the fact that the structural picture of clusters of the form $Sr^+(ND_3)_nD_x$ has both chemical and spectroscopic support, there are a number of important

questions that have not been addressed. For example, the mass spectra indicate that the intensities of clusters with excess numbers of D atoms are larger than those for solvated bare metal ions. The nature of this 'product switching' is yet to be understood. Further evidence for surface bound ND_4 radicals might be obtained from very careful studies of the fragmentation patterns of clusters as they decay. In addition, the metal hydride/deuteride core of such clusters can be probed directly by infrared spectroscopy. Of course, the theoretical challenges these systems afford are severe. Nevertheless, with a careful combination of experimental and theoretical methods, it is reasonable to expect that a clearer picture of these exotic 'multi-Rydberg' species can be obtained.

9. Conclusions

In this review, we have examined the electronic spectroscopy of clusters formed by solvating an effective one-electron core species with polar molecules. All of the spectra exhibit similar, though not identical, behaviour. An array of experimental and theoretical methods on these and related systems suggests that common physics is responsible for the appearance of the spectra. The strong interaction of theory and experiment has demonstrated that a common physical phenomenon, spontaneous ionization, is responsible for the large spectral shifts that are observed in these clusters as their first solvent shells fill. The large red shifts that appear as the first solvation shell fills appear to be related to the role the solvent plays in 'squeezing' the electron into a state that is spatially removed from the valence orbital in which it resides in the cluster core. Many interesting phenomena remain to be observed, and a coherent understanding of such processes will require continuing interactions between experimentalists and theorists addressing issues that are both structural and dynamical in nature. Advances in spectroscopy that allow infrared–optical double resonance probes of the vibrational structures of large clusters in their ground and excited states will play an important role in these studies, as will ultrafast optical methods that probe the timescales for electron and solvent motion. The prospects for using clusters as a vehicle to extend the concepts of gas phase dynamics to condensed phase systems are bright, and we can expect significant advances in these areas in the next few years.

Acknowledgements

The author wishes to thank the following former graduate students for the excellent work they have accomplished in their photodissociation studies of mass-selected cluster ions: Meihua Shen, Stephen Donnelly, Jun Qian, Anthony Midey Jr., David Sperry, and James Lee. The author also acknowledges generous financial support from the National Science Foundation and the Donors of the Petroleum Research Fund of the American Chemical Society.

References

[1] Castleman, A. W., Jr., and Bowen, K. H., Jr., 1996, *J. Phys. Chem.*, **100**, 12911.
[2] Kebarle, P., 1977, *Ann. Rev. Phys. Chem.*, **28**, 445.
[3] Kebarle, P., 1988, 'Pulsed Electron High Pressure Mass Spectrometer'. In *Techniques for the Study of Ion-Molecule Reactions*; Farrar, J. M., Saunders, W. H., Jr., Eds. (New York: Wiley), p. 221.
[4] Kebarle, P., 2000, *Int. J. Mass Spectrom.*, **200**, 313.

[5] Castleman, A. W., Jr., and Keesee, R. G., 1988, *Science*, **241**, 36.
[6] Castleman, A. W., Jr., and Wei, S., 1994, *Ann. Rev. Phys. Chem.*, **45**, 685.
[7] Jena, P., Rao, B. K., and Khanna, S. N., 1986, *Physics and Chemistry of Small Clusters*. In Nato ASI Series, Vol. 158 (New York: Plenum Press).
[8] Rademann, K., Kaiser, B., Even, U., and Hensel, F., 1987, *Phys. Rev. Lett.*, **59**, 2319.
[9] Rademann, K., Dimopoulou-rademann, O., Schlauf, M., Even, U., and Hensel, F., 1992, *Phys. Rev. Lett.*, **69**, 3208.
[10] Delaney, N., Faeder, J., and Parson, R., 1999, *J. Chem. Phys.*, **111**, 452.
[11] Ladanyi, B. M., and Parson, R., 1997, *J. Chem. Phys.*, **107**, 9326.
[12] Nandi, S., Sanov, A., Delaney, N., Faeder, J., Parson, R., and Lineberger, W. C., 1998, *J. Phys. Chem. A*, **102**, 8827.
[13] Parson, R., Faeder, J., and Delaney, N., 2000, *J. Phys. Chem. A*, **104**, 9653.
[14] Stace, A. J., 2001, *Phys. Chem. Chem. Phys.*, **3**, 1935.
[15] Stace, A. J., 2002, *J. Phys. Chem.* A, **106**, 7993.
[16] Frausto da Silva, J. J. R., and Williams, R. J. P., 2001, *Biological Chemistry of the Elements* (New York: Oxford).
[17] Cotton, F. A., and Wilkinson, G., 1988, *Advanced Inorganic Chemistry*, 5th edn (New York: Wiley).
[18] Lisy, J. M., 1997, *Int. Rev. Phys. Chem.*, **16**, 267.
[19] Kleiber, P. D., and Chen, J., 1998, *Int. Rev. Phys. Chem.*, **17**, 1.
[20] Duncan, M. A., 1997, *Ann. Rev. Phys. Chem.*, **48**, 69.
[21] Yeh, C. S., Pilgrim, J. S., Willey, K. F., Robbins, D. L., and Duncan, M. A., 1994, *Int. Rev. Phys. Chem.*, **13**, 231.
[22] Tang, I. N., Lian, M. S., and Castleman, A. W., Jr., 1976, *J. Chem. Phys.*, **65**, 4022.
[23] Andersen, A., Muntean, F., Walter, D., Rue, C., and Armentrout, P. B., 2000, *J. Phys. Chem. A*, **104**, 692.
[24] Qian, J., Midey, A. J., Donnelly, S. G., Lee, J. I., and Farrar, J. M., 1995, *Chem. Phys. Lett.*, **244**, 414.
[25] Sperry, D. C., Midey, A. J., Lee, J. I., Qian, J., and Farrar, J. M., 1999, *J. Chem. Phys.*, **111**, 8469.
[26] Lee, J. I., Sperry, D. C., and Farrar, J. M., 2001, *J. Chem. Phys.*, **114**, 6180.
[27] Lee, J. I., and Farrar, J. M., 2002, *J. Phys. Chem. A*, **106**, 11882.
[28] Lee, J. I., Qian, J., Sperry, D. C., Midey, A. J., Donnelly, S. G., and Farrar, J. M., 2002, *J. Phys. Chem. A*, **106**, 9993.
[29] Fuke, K., Misaizu, F., Sanekata, M., Tsukamoto, K., and Iwata, S., 1993, *Z. Phys. D-Atoms Mol. Clusters*, **26**, S180.
[30] Lu, W., and Yang, S., 1998, *J. Phys. Chem. A*, **102**, 825.
[31] Misaizu, F., Sanekata, M., Tsukamoto, K., and Fuke, K., 1992, *J. Phys. Chem.*, **96**, 8259.
[32] Misaizu, F., Sanekata, M., and Fuke, K., 1994, *J. Chem. Phys.*, **100**, 1161.
[33] Sanekata, M., Misaizu, F., Fuke, K., Iwata, S., and Hashimoto, K., 1995, *J. Am. Chem. Soc.*, **117**, 747.
[34] *The Chemical Physics of Solvation*, Part C, 1988, Dogonadze, R. R., Kalman, E., Kornyshev, A. A., and Ulstrup, J., Eds. (Amsterdam: Elsevier).
[35] Tuttle, T. R., and Golden, S., 1991, *J. Phys. Chem.*, **95**, 5725.
[36] Gregoire, G., Brinkmann, N. R., van Heijnsbergen, D., Schaefer, H. F., and Duncan, M. A., 2003, *J. Phys. Chem. A*, **107**, 218.
[37] Pilgrim, J. S., Yeh, C. S., and Duncan, M. A., 1993, *Chem. Phys. Lett.*, **210**, 322.
[38] Pilgrim, J. S., Yeh, C. S., Berry, K. R., and Duncan, M. A., 1994, *J. Chem. Phys.*, **100**, 7945.
[39] Pullins, S. H., Scurlock, C. T., Reddic, J. E., and Duncan, M. A., 1996, *J. Chem. Phys.*, **104**, 7518.
[40] Reddic, J. E., Pullins, S. H., and Duncan, M. A., 2000, *J. Chem. Phys.*, **112**, 4974.
[41] Scurlock, C. T., Pilgrim, J. S., and Duncan, M. A., 1995, *J. Chem. Phys.*, **103**, 3293.
[42] Scurlock, C. T., Pilgrim, J. S., and Duncan, M. A., 1996, *J. Chem. Phys.*, **105**, 7876.

[43] Fanourgakis, G. S., Farantos, S. C., Luder, C., Velegrakis, M., and Xantheas, S. S., 1998, *J. Chem. Phys.*, **109**, 108.
[44] Fanourgakis, G. S., Farantos, S. C., Luder, C., Velegrakis, M., and Xantheas, S. S., 1999, *Phys. Chem. Chem. Phys.*, **1**, 977.
[45] Luder, C., and Velegrakis, M., 1996, *J. Chem. Phys.*, **105**, 2167.
[46] Luder, C., Prekas, D., and Velegrakis, M., 1997, *Laser Chem.*, **17**, 109.
[47] Luder, C., Prekas, D., Vourliotaki, A., and Velegrakis, M., 1997, *Chem. Phys. Lett.*, **267**, 149.
[48] Lüder, C., and Velegrakis, M., 1996, *J. Chem. Phys.*, **105**, 2167.
[49] Prekas, D., Feng, B. H., and Velegrakis, M., 1998, *J. Chem. Phys.*, **108**, 2712.
[50] Velegrakis, M., and Luder, C., 1994, *Chem. Phys. Lett.*, **223**, 139.
[51] Xantheas, S. S., Fanourgakis, G. S., Farantos, S. C., and Velegrakis, M., 1998, *J. Chem. Phys.*, **108**, 46.
[52] Cornett, D. S., Peschke, M., Laihing, K., Cheng, P. Y., Willey, K. F., and Duncan, M. A., 1992, *Rev. Sci. Instrum.*, **63**, 2177.
[53] Donnelly, S. G., and Farrar, J. M., 1993, *J. Chem. Phys.*, **98**, 5450.
[54] Donnelly, S. G., 1994, *Photodissociation Studies of Mass Selected Clusters*. Doctoral Dissertation, University of Rochester.
[55] Alexander, M. L., Johnson, M. A., Levinger, N. E., and Lineberger, W. C., 1986, *Phys. Rev. Lett.*, **57**, 976.
[56] Alexander, M. L., Levinger, N. E., Johnson, M. A., Ray, D., and Lineberger, W. C., 1988, *J. Chem. Phys.*, **88**, 6200.
[57] Levinger, N. E., Ray, D., Alexander, M. L., and Lineberger, W. C., 1988, *J. Chem. Phys.*, **89**, 5654.
[58] Posey, L. A., Deluca, M. J., and Johnson, M. A., 1986, *Chem. Phys. Lett.*, **131**, 170.
[59] Dietz, T. G., Duncan, M. A., Powers, D. E., and Smalley, R. E., 1981, *J. Chem. Phys.*, **74**, 6511.
[60] Wiley, W. C., and McLaren, I. H., 1955, *Rev. Sci. Instrum.*, **26**, 1150.
[61] Mamyrin, B. A., Karatev, V. I., Schmikk, D. V., and Zagulin, V. A., 1973, *Sov. Phys. JETP*, **37**, 45.
[62] Lorquet, J. C., and Leyh, B., 2003, 'Statistical Theories of Mass Spectrometry'. In *The Encyclopedia of Mass Spectrometry Volume 1: Theory and Ion Chemistry*; Armentrout, P. B., Ed. (Amsterdam: Elsevier), p. 8.
[63] Sperry, D. C., Lee, J. I., and Farrar, J. M., 1999, *Chem. Phys. Lett.*, **304**, 350.
[64] Yoshida, S., Okai, N., and Fuke, K., 2001, *Chem. Phys. Lett.*, **347**, 93.
[65] Yoshida, S., Daigoku, K., Okai, N., Takahata, A., Sabu, A., Hashimoto, K., and Fuke, K., 2002, *J. Chem. Phys.*, **117**, 8657.
[66] Bauschlicher, C. W., Jr., Sodupe, M., and Partridge, H., 1992, *J. Chem. Phys.*, **96**, 4453.
[67] Qian, J., 1995, *Photodissociation Studies of Size-Selected Solvated Strontium Cation Clusters*. Doctoral Dissertation, University of Rochester.
[68] Davis, H. F., Suits, A. G., Lee, Y. T., Alcaraz, C., and Mestdagh, J.-M., 1993, *J. Chem. Phys.*, **98**, 9595.
[69] Low, J. J., and Goddard, W. A., 1986, *J. Am. Chem. Soc.*, **108**, 6115.
[70] Low, J. J., and Goddard, W. A., 1984, *J. Am. Chem. Soc.*, **106**, 8321.
[71] Sulzbach, H. M., Platz, M. S., Schaefer, H. F., III, and Hadad, C. M., 1997, *J. Am. Chem. Soc.*, **119**, 5682.
[72] Sanekata, M., Misaizu, F., and Fuke, K., 1996, *J. Chem. Phys.*, **104**, 9768.
[73] France, M. R., Pullins, S. H., and Duncan, M. A., 1998, *Chem. Phys.*, **239**, 447.
[74] Woodward, C. A., Dobson, M. P., and Stace, A. J., 1997, *J. Phys. Chem. A*, **101**, 2279.
[75] Misaizu, F., Sanekata, M., Fuke, K., and Iwata, S., 1994, *J. Chem. Phys.*, **100**, 1161.
[76] Shen, M. H., and Farrar, J. M., 1989, *J. Phys. Chem.*, **93**, 4386.
[77] Shen, M. H., and Farrar, J. M., 1991, *J. Chem. Phys.*, **94**, 3322.
[78] Rice, S. F., Martin, H., and Field, R. W., 1985, *J. Chem. Phys.*, **82**, 5023.
[79] Shen, M., Winniczek, J. W., and Farrar, J. M., 1987, *J. Phys. Chem.*, **91**, 6447.
[80] Thompson, J. C., 1976, *Electrons in Liquid Ammonia* (Oxford: Oxford Press).

[81] Sanekata, M., Misaizu, F., and Fuke, K., 1996, *J. Chem. Phys.*, **104**, 9768.
[82] Sanekata, M., Misaizu, F., Fuke, K., Iwata, S., and Hashimoto, K., 1995, *J. Am. Chem. Soc.*, **117**, 747.
[83] Kochanski, E., and Constantin, E., 1987, *J. Chem. Phys.*, **87**, 1661.
[84] Willey, K. F., Yeh, C. S., Robbins, D. L., Pilgrim, J. S., and Duncan, M. A., 1992, *J. Chem. Phys.*, **97**, 8886.
[85] Yeh, C. S., Willey, K. F., Robbins, D. L., Pilgrim, J. S., and Duncan, M. A., 1992, *Chem. Phys. Lett.*, **196**, 233.
[86] Misaizu, F., Sanekata, M., Tsukamoto, K., Fuke, K., and Iwata, S., 1992, *J. Phys. Chem.*, **96**, 8259.
[87] Sodupe, M., and Bauschlicher, C. W., Jr., 1992, *Chem. Phys. Lett.*, **195**, 494.
[88] Watanabe, H., and Iwata, S., 1998, *J. Chem. Phys.*, **108**, 10078.
[89] Fuke, K., Hashimoto, K., and Iwata, S., 1999, 'Structures, spectroscopies, and reactions of atomic ions with water clusters'. In *Advances in Chemical Physics*, Vol. 110 (New York: Wiley-Interscience), p. 431.
[90] Watanabe, H., and Iwata, S., 1997, *J. Phys. Chem. A*, **101**, 487.
[91] Lee, J. I., Sperry, D. C., and Farrar, J. M. (in preparation).
[92] Reinhard, B. M., and Niedner-Schatteburg, G., 2002, *Phys. Chem. Chem. Phys.*, **4**, 1471.
[93] Reinhard, B. M., and Niedner-Schatteburg, G., 2003, *Phys. Chem. Chem. Phys.*, **5**, 1970.
[94] Reinhard, B. M., and Niedner-Schatteburg, G., 2003, *J. Chem. Phys.*, **118**, 3571.
[95] Milburn, R. K., Baranov, V. I., Hopkinson, A. C., and Bohme, D. K., 1998, *J. Phys. Chem. A*, **102**, 9803.
[96] Milburn, R. K., Bohme, D. K., and Hopkinson, A. C., 2001, *J. Mol. Struct.-Theochem*, **540**, 5.
[97] Elhanine, M., Dukan, L., Maitre, P., Breckenridge, W. H., Massick, S., and Soep, B., 2000, *J. Chem. Phys.*, **112**, 10912.
[98] Brockhaus, P., Hertel, I. V., and Schulz, C. P., 1999, *J. Chem. Phys.*, **110**, 393.
[99] Hashimoto, K., He, S., and Morokuma, K., 1993, *Chem. Phys. Lett.*, **206**, 297.
[100] Hashimoto, K., and Morokuma, K., 1995, *J. Am. Chem. Soc.*, **117**, 4151.
[101] Herzberg, G., 1981, *Faraday Discuss. Chem. Soc.*, **71**, 165.
[102] Alberti, F., Huber, K. P., and Watson, J. K. G., 1984, *J. Mol. Spectrosc.*, **107**, 133.
[103] Gellene, G. I., Cleary, D. A., and Porter, R. F., 1982, *J. Chem. Phys.*, **77**, 3471.
[104] Williams, B. W., and Porter, R. F., 1980, *J. Chem. Phys.*, **73**, 5598.
[105] Misaizu, F., Houston, P. L., Nishi, N., Shinohara, H., Kondow, T., and Kinoshita, M., 1993, *J. Chem. Phys.*, **98**, 336.
[106] Gellene, G. I., and Porter, R. F., 1984, *J. Phys. Chem.*, **88**, 6680.
[107] Gellene, G. I., and Porter, R. F., 1985, *Int. J. Mass Spectrom. Ion Processes*, **64**, 55.
[108] Fuke, K., Takasu, R., and Misaizu, F., 1994, *Chem. Phys. Lett.*, **229**, 597.
[109] Takasu, R., Fuke, K., and Misaizu, F., 1996, *Surf. Rev. Lett.*, **3**, 353.
[110] Nonose, S., Taguchi, T., Mizuma, K., and Fuke, K., 1999, *Eur. Phys. J. D*, **9**, 309.
[111] Nonose, S., Taguchi, T., Chen, F. W., Iwata, S., and Fuke, K., 2002, *J. Phys. Chem. A*, **106**, 5242.
[112] Daigoku, K., Miura, N., and Hashimoto, K., 2001, *Chem. Phys. Lett.*, **346**, 81.
[113] Rodgers, M. T., and Armentrout, P. B., 1997, *J. Phys. Chem. A*, **101**, 1238.
[114] Walter, D., and Armentrout, P. B., 1998, *J. Am. Chem. Soc.*, **120**, 3176.
[115] Bauschlicher, C. W., Jr., and Partridge, H., 1991, *J. Phys. Chem.*, **95**, 3946.
[116] Bauschlicher, C. W., Jr., and Partridge, H., 1991, *J. Phys. Chem.*, **95**, 9694.
[117] Bauschlicher, C. W., Jr., and Partridge, H., 1991, *Chem. Phys. Lett.*, **181**, 129.
[118] Bauer, E., Fisher, E. R., and Gilmore, F. R., 1969, *J. Chem. Phys.*, **51**, 4173.
[119] Polanyi, M., 1932, *Atomic Reactions* (London: Williams and Norgate).
[120] Herschbach, D. R., 1966, 'Reactive Scattering in Molecular Beams'. In *Molecular Beams*; Ross, J., Ed. (New York: Interscience Publishers), p. 319.
[121] Hertel, I. V., 1982, 'Progress in Electronic-to-Vibrational Energy Transfer'. In *Dynamics of the Excited State*; Lawley, K. P., Ed. (New York: Wiley-Interscience), p. 475.
[122] Aten, J. A., and Los, J., 1977, *Chem. Phys.*, **25**, 47.

[123] Habitz, P., 1980, *Chem. Phys.*, **54**, 131.
[124] Chen, J., Cheng, Y. C., and Kleiber, P. D., 1997, *J. Chem. Phys.*, **106**, 3884.
[125] Chen, J., Wong, T. H., Cheng, Y. C., Montgomery, K., and Kleiber, P. D., 1998, *J. Chem. Phys.*, **108**, 2285.
[126] Cheng, Y. C., Chen, J., Ding, L. N., Wong, T. H., Kleiber, P. D., and Liu, D.-K., 1998, *J. Chem. Phys.*, **104**, 6452.
[127] Wong, T. H., Freel, C., and Kleiber, P. D., 1998, *J. Chem. Phys.*, **108**, 5723.
[128] Crim, F. F., 1990, *Science*, **249**, 1387.
[129] Crim, F. F., 1993, *Ann. Rev. Phys. Chem.*, **44**, 397.
[130] Crim, F. F., 1996, *J. Phys. Chem.*, **100**, 12725.
[131] Crim, F. F., 1999, *Acc. Chem. Res.*, **32**, 877.
[132] Takasu, R., Hashimoto, K., and Fuke, K., 1996, *Chem. Phys. Lett.*, **258**, 94.
[133] Misaizu, F., Tsukamoto, K., Sanekata, M., and Fuke, K., 1992, *Chem. Phys. Lett.*, **188**, 241.
[134] Takasu, R., Misaizu, F., Hashimoto, K., and Fuke, K., 1997, *J. Phys. Chem. A*, **101**, 3078.
[135] Hertel, I. V., Huglin, C., Nitsch, C., and Schulz, C. P., 1991, *Phys. Rev. Lett.*, **67**, 1767.
[136] Brus, L. E., 1983, *J. Chem. Phys.*, **79**, 5566.
[137] Brus, L. E., 1984, *J. Chem. Phys.*, **80**, 4403.
[138] Barnett, R. N., Landman, U., Cleveland, C. L., and Jortner, J., 1988, *Chem. Phys. Lett.*, **145**, 382.
[139] Stampfli, P., and Bennemann, K. H., 1987, *Phys. Rev. Lett.*, **58**, 2635.
[140] Stampfli, P., and Bennemann, K. H., 1992, *Ber. Bunsen-Ges. Phys. Chem. Chem. Phys.*, **96**, 1220.
[141] Aulich, H., Baron, B., Delahay, P., and Lugo, R., 1973, *J. Chem. Phys.*, **58**, 4439.
[142] Coe, J. V., Lee, G. H., Eaton, J. G., Arnold, S. T., Sarkas, H. W., Bowen, K. H., Ludewigt, C., Haberland, H., and Worsnop, D. R., 1990, *J. Chem. Phys.*, **92**, 3980.
[143] Sarkas, H. W., Arnold, S. T., Eaton, J. G., Lee, G. H., and Bowen, K. H., 2002, *J. Chem. Phys.*, **116**, 5731.
[144] Lee, G. H., Arnold, S. T., Eaton, J. G., Sarkas, H. W., Bowen, K. H., Jr., Ludewigt, C., and Haberland, H., 1991, *Z. Phys. D*, **20**, 9.
[145] Cohan, N. V., Finkelstein, G., and Weissmann, M., 1974, *Chem. Phys. Lett.*, **26**, 93.
[146] Barnett, R. N., Landman, U., Cleveland, C. L., Kestner, N. R., and Jortner, J., 1988, *J. Chem. Phys.*, **88**, 6670.
[147] Barnett, R. N., Landman, U., Cleveland, C. L., and Jortner, J., 1988, *J. Chem. Phys.*, **88**, 4429.
[148] Harrison, J. A., Isakson, L. J., and Mayne, H. R., 1989, *J. Chem. Phys.*, **91**, 6906.
[149] Hashimoto, K., and Morokuma, K., 1994, *J. Am. Chem. Soc.*, **116**, 11436.
[150] Hashimoto, K., and Morokuma, K., 1994, *Chem. Phys. Lett.*, **223**, 423.
[151] Tsurusawa, T., and Iwata, S., 1999, *J. Phys. Chem. A*, **103**, 6134.
[152] Kim, K. S., Lee, S., Kim, J., and Lee, J. Y., 1997, *J. Am. Chem. Soc.*, **119**, 9329.
[153] Lee, S., Kim, J., Lee, S. J., and Kim, K. S., 1997, *Phys. Rev. Lett.*, **79**, 2038.
[154] Bailey, C. G., Kim, J., and Johnson, M. A., 1996, *J. Phys. Chem.*, **100**, 16782.
[155] Franck, J., and Platzman, R., 1954, *Z. Phys.*, **138**, 411.
[156] Blandamer, M. J., and Fox, M. F., 1970, *Chem. Rev.*, **70**, 59.
[157] Martyna, G. J., and Klein, M. L., 1991, *J. Phys. Chem.*, **95**, 515.
[158] Rencsok, R., Kaplan, T. A., and Harrison, J. F., 1993, *J. Chem. Phys.*, **98**, 9758.
[159] Fano, U., and Cooper, J. W., 1968, *Rev. Mod. Phys.*, **40**, 441.
[160] Berkowitz, J., 1979, *Photoabsorption, Photoionization, and Photoelectron Spectroscopy* (New York: Academic Press).
[161] Campagnola, P. J., Lavrich, D. J., and Johnson, M. A., 1991, *J. Phys. IV*, **1**, 93.
[162] Campagnola, P. J., Posey, L. A., and Johnson, M. A., 1991, *J. Chem. Phys.*, **95**, 7998.
[163] Campagnola, P. J., Cyr, D. M., and Johnson, M. A., 1991, *Chem. Phys. Lett.*, **181**, 206.

[164] Hashimoto, K., Kamimoto, T., Miura, N., Okuda, R., and Daigoku, K., 2000, *J. Chem. Phys.*, **113**, 9540.
[165] Hashimoto, K., Kamimoto, T., and Daigoku, K., 2000, *J. Phys. Chem. A*, **104**, 3299.
[166] Fuentealba, P., and Reyes, O., 1987, *Mol. Phys.*, **62**, 1291.
[167] Schilling, J. B., Goddard, W. A., III, and Beauchamp, J. L., 1987, *J. Am. Chem. Soc.*, **109**, 5565.
[168] Ohanessian, G., and Goddard, W. A., III, 1990, *Acc. Chem. Res.*, **23**, 386.
[169] Dalleska, N. F., Crellin, K. C., and Armentrout, P. B., 1993, *J. Phys. Chem.*, **97**, 3123.
[170] Kaupp, M., Schleyer, P. V. R., Stoll, H., and Preuss, H., 1991, *J. Chem. Phys.*, **94**, 1360.
[171] Huber, K. P., and Herzberg, G., 1979, *Constants of Diatomic Molecules* (New York: Van Nostrand).
[172] Boutalib, A., Daudey, J. P., and Elmouhtadi, M., 1992, *Chem. Phys.*, **167**, 111.
[173] Purnell, J., Snyder, E. M., Wei, S., and Castleman, A. W., Jr., 1994, *Chem. Phys. Lett.*, **229**, 333.
[174] Snyder, E. M., Purnell, J., Wei, S., Buzza, S. A., and Castleman, A. W., 1996, *Chem. Phys.*, **207**, 355.
[175] Wei, S., Purnell, J., Buzza, S. A., and Castleman, A. W., 1993, *J. Chem. Phys.*, **99**, 755.
[176] Boldyrev, A. I., and Simons, J., 1999, *J. Phys. Chem. A*, **103**, 3575.